EFFECT OF GRAIN SIZE AND MICROPOROSITY ON THE *IN VIVO* BEHAVIOUR OF β-TRICALCIUM PHOSPHATE SCAFFOLDS

H. Lapczyna[1], L. Galea[2], S. Wüst[3], M. Bohner[2,]*, S. Jerban[4], A. Sweedy[4], N. Doebelin[2], N. van Garderen[2], S. Hofmann[3,5,6], G. Baroud[4], R. Müller[3] and B. von Rechenberg[1]

[1]Musculoskeletal Research Unit (MSRU), Competence Center for Applied Biotechnology and Molecular Medicine (CABMM), Equine Hospital, University of Zurich, Zurich, Switzerland
[2]RMS Foundation, Bettlach, Switzerland
[3]Institute for Biomechanics, ETH Zurich, Zurich, Switzerland
[4]Laboratoire de Biomécanique, Département de Génie, Université de Sherbrooke, Sherbrooke, Québec, Canada J1K 2R1
[5]Department of Biomedical Engineering, Eindhoven University of Technology, Eindhoven, The Netherlands
[6]Institute for Complex Molecular Systems, Eindhoven University of Technology, Eindhoven, The Netherlands

Abstract

Defining the most adequate architecture of a bone substitute scaffold is a topic that has received much attention over the last 40 years. However, contradictory results exist on the effect of grain size and microporosity. Therefore, the aim of this study was to determine the effect of these two factors on the *in vivo* behaviour of β-tricalcium phosphate (β-TCP) scaffolds. For that purpose, β-TCP scaffolds were produced with roughly the same macropore size (≈ 150 μm), and porosity (≈ 80 %), but two levels of microporosity (low: 10 % / high: ≈ 25 %) and grain size (small: 1.3 μm /large: ≈ 3.3 μm). The sample architecture was characterised extensively using materialography, Hg porosimetry, micro-computed tomography (μCT), and nitrogen adsorption. The scaffolds were implanted for 2, 4 and 8 weeks in a cylindrical 5-wall cancellous bone defect in sheep. The histological, histomorphometrical and μCT analysis of the samples revealed that all four scaffold types were almost completely resorbed within 8 weeks and replaced by new bone. Despite the three-fold difference in microporosity and grain size, very few biological differences were observed. The only significant effect at $p < 0.01$ was a slightly faster resorption rate and soft tissue formation between 4 and 8 weeks of implantation when microporosity was increased. Past and present results suggest that the biological response of this particular defect is not very sensitive towards physico-chemical differences of resorbable bone graft substitutes. As bone formed not only in the macropores but also in the micropores, a closer study at the microscopic and localised effects is necessary.

Keywords: Resorption, bone graft, calcium phosphate, microstructure, porosity, scaffold, tricalcium phosphate, micropore, grain, size.

*Address for correspondence:
Marc Bohner
RMS Foundation, Bischmattstrasse 12
CH-2544 Bettlach, Switzerland

Telephone Number: +41 32 6441413
FAX Number: +41 32 6441176
E-mail: marc.bohner@rms-foundation.ch

Introduction

Synthetic bone graft substitutes (BGSs) have been increasingly used over the past 40 years as replacement for autologous bone grafts (Klawitter and Hulbert, 1971; Hench, 2006). Intensive efforts have been made to determine the most adequate composition and architecture. On the chemical side, many materials varying in composition and architecture have been proposed, including polymers (Ishaug-Riley *et al.*, 1997; Ignatius *et al.*, 2001; Mondrinos *et al.*, 2006; Gogolewski *et al.*, 2008), metals (Ayers *et al.*, 1999; Bobyn *et al.*, 1999; Itala *et al.*, 2001; Witte *et al.*, 2007) and ceramics (Klawitter and Hulbert, 1971; Klein *et al.*, 1985; van Blitterswijk *et al.*, 1986; Eggli *et al.*, 1988; Daculsi and Passuti, 1990; Schliephake *et al.*, 1991; Basle *et al.*, 1993; Metsger *et al.*, 1993; Lu *et al.*, 1999; Flautre *et al.*, 2001; Walsh *et al.*, 2003; Jones and Hench, 2004; Linhart *et al.*, 2004; Hench, 2006; Von Doernberg *et al.*, 2006; Mastrogiacomo *et al.*, 2007; Lan Levengood *et al.*, 2010; Murakami *et al.*, 2010; Yuan *et al.*, 2010; Polak *et al.*, 2011; Haugen *et al.*, 2013). These materials present very different resorption rates, and many resorption mechanisms, such as dissolution, hydrolysis (*e.g.*, poly(α-hydroxy acids) (Ignatius *et al.*, 2001)), cell-mediated resorption (Basle *et al.*, 1993; Lu *et al.*, 1999; Von Doernberg *et al.*, 2006; Yuan *et al.*, 2010), corrosion (Witte *et al.*, 2007), enzymatic degradation (Hutmacher, 2000; Vert, 2007), and transport (Vert, 2007).

Beside chemical effects, architectural aspects have also been considered to be crucial for the *in vivo* response. These include porosity (Klein *et al.*, 1985; Metsger *et al.*, 1993), pore size (Klawitter and Hulbert, 1971; van Blitterswijk *et al.*, 1986; Eggli *et al.*, 1988; Daculsi and Passuti, 1990; Schliephake *et al.*, 1991; Metsger *et al.*, 1993; Ayers *et al.*, 1999; Itala *et al.*, 2001; von Doernberg *et al.*, 2006; Chan *et al.*, 2012), interconnection pore size (Lu *et al.*, 1999; Flautre *et al.*, 2001) or granule size (Malard *et al.*, 1999; Murakami *et al.*, 2010). Microscopic features such as micropores or crystal grain size have also been the subject of investigations (Klein *et al.*, 1983; Klein *et al.*, 1984; Klein *et al.*, 1985; Klein *et al.*, 1986; De Groot, 1988; De Groot *et al.*, 1988; Van der Meulen and Koerten, 1994; Gauthier *et al.*, 1999; Lan Levengood *et al.*, 2010; Wei *et al.*, 2010; Yuan *et al.*, 2010; Campion *et al.*, 2011; Chan *et al.*, 2012; Coathup *et al.*, 2012) (Table 1). For example, Wei *et al*. (Wei *et al.*, 2010) implanted magnesium-calcium phosphate macroporous scaffolds with

Table 1. List in alphabetical order of several studies devoted to the effect of architectural factors on the *in vivo* performance of resorbable calcium phosphate ceramic scaffolds (sintered hydroxyapatite is considered to be non-resorbable). Various aspects were considered: micro and macropore size, Micro and macroporosity, grain size, pore interconnection size. Abbreviations: d = days; w = weeks; m = months; NA = not applicable / no response; MPor = macroporosity; μPor = microporosity.

Author	Animal model (Implantation time)	Material	Investigated factor(s)	Resorption	Bone formation	Remarks
Bai *et al.* (Bai *et al.*, 2010)	Rabbits (1, 2, 4, 8 w)	β-TCP	Macropore size and Interconnection size MPor size: 300-400, 400-500, 500-600, 600-700 μm; interconnection: from 72 to 198 μm; porosity: 67-79 %	NA	NA	Increase of blood vessel ingrowth with an increase of macropore and interconnection size
Feng *et al.* (Feng *et al.*, 2011)	Rabbits (1, 2, 4, 8 w)	β-TCP	Macropore size MPor size: 300-400, 400-500, 500-600, 600-700 μm; interconnection ≈ 120 μm; porosity ≈ 72 %	NA	NA	Decrease of fibrous tissue ingrowth and increase of blood vessel ingrowth with an increase of macropore size
Eggli *et al.* (Eggli *et al.*, 1988)	Rabbits (2, 4 w, 4, 6 m)	β-TCP	Macropore size MPor size: group 1: 50-100, Group 2: 200-400 μm.	2/3 and 5/6 resorbed after 6 months for group I and II, resp.	≈ 2x faster in group I than group II at 2 and 4 weeks	Very limited material characterization
Gauthier *et al.* (Gauthier *et al.*, 1999)	Rabbits (8 w)	BCP	Grain size Two groups produced according to the same method but with two different raw materials	Fourfold increase of resorption rate with an increase of grain size	No difference	No grain size measurement. Group 1: roughly 1 μm grain size; Group 2: 0.1-0.2 μm grain size. Not the same raw material for the two groups. No 3D characterization of the architecture.
Hong *et al.* (Hong *et al.*, 2010)	Dogs (45, 90 d)	BCP	Grain size Two groups; Difference of grain size between group 1 (86 ± 20 nm) and group 2 (768 ± 321 nm)	NA	10-20 % more bone formation in group 1	
Kasten *et al.* (Kasten *et al.*, 2008)	SCID Mice (8 w)	β-TCP	Porosity Three groups with 25, 65 and 75 % porosity	NA	*In vivo* ALP activity highest with 65 % porosity, lowest with 25 % porosity	"Higher porosity does not necessarily mean higher ALP activity *in vivo*"
Klein *et al.* (Klein *et al.*, 1985)	Rabbits (16 m)	β-TCP	Microporosity and Macroporosity Four groups without or with macropores, and with a small (< 5 %) and large (50-60 %) amount of micropores	Faster resorption of the microporous samples	More bone ingrowth in the macroporous samples	Only qualitative results. Only one histological time point (16 months). Only XRD to assess resorption within the first months of implantation
Klein *et al.* (Klein *et al.*, 1983)	Rabbits (3, 6, 9 m)	β-TCP	Microporosity and Macroporosity Group 1: MPor: 0 %; μPor: 2 %; Group 2: MPor: 0 %; μPor: 40 %; Group 3: MPor: 30 %; μPor: 2 %; Group 4: MPor: 30 %; μPor: 40 %;	Faster with more macroporosity and microporosity	NA	Only qualitative results. De Groot mentioned a degradation rate at 3 months of 15 % and 30 % for groups 3 and 4 (De Groot, 1988). *In vitro* dissolution data in (Klein *et al.*, 1984), in line with *in vivo* results.
Klein *et al.* (Klein *et al.*, 1986)	Rabbits (3, 6, 12 m)	β-TCP	Microporosity and Macroporosity 5 groups; Microporosity between 40 and 55 %; Macroporosity between 0 and 20 %.	Faster with more macroporosity and microporosity	No difference	Only qualitative results.
Metsger (Metsger *et al.*, 1993)	Turkeys (2, 4, 6 m)	β-TCP	Macroporosity and Porosity "two pore size distributions and four pore densities"	Qualitatively, slightly faster resorption in smaller pores	Qualitatively, slightly faster bone ingrowth in smaller pores	Not clear how many materials were tested and how they differed. Observation of a coupling between resorption and bone formation
Okuda *et al.* (Okuda *et al.*, 2007)	Rabbits (2, 4, 12, 24 w)	β-TCP	Microstructure Fiber-like and sintered-like structure. μPor size: 0.2 μm and 0.5 μm respectively. Porosity: 70 %	No difference within the first 12 weeks	No difference within the first 12 weeks	
Von Doernberg *et al.* (von Doernberg *et al.*, 2006)	Sheep (6, 12, 24 w)	β-TCP	Macropore size MPor size: 150, 260, 510, 1220 μm; μPor ≈ 21 %; MPor ≈ 54 %, Porosity ≈ 75 %	Almost no difference	No difference	
Wei *et al.* (Wei *et al.*, 2010)	Rabbits (1, 2, 3, 6 m)	PHA[1] MAP[2]	Macroporosity Both materials produced without and with macropores. Porosity: 52-78 %. MPor size: 400-500 μm.	NA	More bone in the macroporous samples, but only at 3 and 6 months implantation	
Yokozeki *et al.* (Yokozeki *et al.*, 1998)	Rabbits (4, 12, 24 w)	β-TCP	Microporosity Group 1: μPor ≈ NA; μPor size ≈ 0.2-0.5 μm; Porosity ≈ 60 % ; MPor size: 150-400 μm; SSA = 10 m²/g); Group 2: μPor ≈ 0 %; Porosity ≈ 57 % ; MPor size: 150-400 μm; SSA = 2 m²/g	-30 % in ceramic area at 24 w for group 1; -2 % for group 2	No difference Very small amount of bone	Not clear how a ceramic with 0 % microporosity can have a SSA value of 2 m²/g. No XRD data demonstrating that both ceramics are pure β-TCP. Not the same raw materials for the two groups.

9 and 27 % microporosity and observed that the presence of micropores increased the degradation rate and accelerated bone formation. A similar result was found by Yokozeki *et al.* (Yokozeki *et al.*, 1998) and the group of De Groot (Klein *et al.*, 1983; Klein *et al.*, 1984; Klein *et al.*, 1985; Klein *et al.*, 1986; De Groot, 1988). Klein *et al.* (Klein *et al.*, 1985) suggested that changes of microporosity degree played a more important role in the resorption process than changes in macroporosity degree. Lan Levengood *et al.* (Lan Levengood *et al.*, 2010) stated that "the exploitation of microporosity to achieve multiscale osteointegration offers a new paradigm for scaffold design". More recently, the presence of micropores was associated with the osteoinductive potential of calcium phosphate (CaP) ceramics (Yuan *et al.*, 2010; Chan *et al.*, 2012; Coathup *et al.*, 2012), and a change in cell and bone ingrowth (Lan Levengood *et al.*, 2010; Polak *et al.*, 2013). Regarding grain size, grain boundaries were found to be attacked during resorption, leading to particle release (Van der Meulen and Koerten, 1994). Klein *et al.* mentioned that this localised dissolution controls resorption (Klein *et al.*, 1984) and that the dimensions and composition of the grain boundary

(= neck) affect their resorption (Klein *et al.*, 1986). Also, dissolution-precipitation reactions that are involved during calcium phosphate resorption (LeGeros, 1993; Koerten and van der Meulen, 1999; LeGeros, 2002; Le Nihouannen *et al.*, 2005) were seen to occur between partly dissolved grains (Van der Meulen and Koerten, 1994). LeGeros *et al.* (LeGeros *et al.*, 1988) and Klein *et al.* (Klein *et al.*, 1983; Klein *et al.*, 1986) observed an increase in resorption rate with a decrease in grain size.

Even though most studies devoted to microscopic features suggest that an increase of microporosity and a decrease of grain size accelerate resorption, it is difficult to draw conclusions for two reasons. First, it is very difficult to vary one parameter (*e.g.*, micropore size) without changing other parameters (*e.g.*, porosity). As a result, most studies on the topic contain rather fragmentary microstructural characterisations. Second, contradictory results exist. For example, Gauthier *et al.* (Gauthier *et al.*, 1999) implanted biphasic CaPs and observed a fourfold decrease of degradation rate with an about fivefold decrease of grains / micropores. Therefore, the aim of the present study was to determine quantitatively the effect of a change of microporosity and grain size on the *in vivo* behaviour of β-TCP scaffolds. Compared to published studies, extensive investigations were performed prior to the study to design scaffolds varying independently in microporosity and grain size. Also in depth characterisations were performed to give a precise description of the four implanted scaffold types, in particular porosity, pore size (from the nano to the macroscale), and grain size. Finally, the 3D geometry was determined before and after implantation to eventually be able to apply a resorption model on the data (Bohner and Baumgart, 2004).

In this article, nanopores were considered to be pores with diameters smaller than 100 nm. Micropores were defined as pores with diameters ranging between 100 nm and 50 μm. Finally, macropores were considered to have a diameter larger than 50 μm, as it is generally recognised that an interconnection size close to 50 μm is essential for bone ingrowth (Karageorgiou and Kaplan, 2005).

Materials and Methods

To investigate the effect of microporosity and grain size on the *in vivo* behaviour of β-TCP scaffolds, four types of macroporous β-TCP scaffolds were produced according to a 2 x 2 factorial design of experiment: (i) low microporosity and small grain size (denominated "mg": "m" for a low microporosity and "g" for a small grain size), (ii) high microporosity and small grain size ("M" for high microporosity; "Mg"), (iii) low microporosity and large grain size ("G" for large grain size; "mG"), and (iv) high microporosity and large grain size ("MG"). For that purpose, two α-TCP powders, two blend compositions, and two sintering profiles were selected. The next paragraphs describe the synthesis procedure in more details.

Raw material synthesis
α-tricalcium phosphate (α-TCP; α-$Ca_3(PO_4)_2$) was produced according to a procedure previously described

(Bohner *et al.*, 2009). The powder was then processed in two ways: (i) planetary milling (Pulverisette 5, Fritsch, Idar-Oberstein, Germany) for 2 h with 10 % fumaric acid (Lot #BCBB8136, Art 47910, Fluka/Sigma-Aldrich, St. Louis, MO, USA) and 2 mL ethanol (100 g α-TCP powder, 500 mL jars, 100 ZrO_2 beads (= 300 g)), followed by calcination at 500 °C for 12 h; this powder was used to produce mg and Mg samples; (ii) ball milling at 60 rpm for 6 h in ethanol (555 ± 5 g powder, 420 ± 4 g ethanol, 5505 ± 10 g ZrO_2 beads; 2L polyethylene (PE) bottles), drying in air and then calcination at 500 °C for 1 h and later on at 700 °C for 1 h; this powder was used to produce mG and MG samples.

Scaffold synthesis
All scaffolds were produced by isostatically pressing a mixture of α-TCP powder, stearic acid (Merck, Darmstadt, Germany; 1.00661.9020), and polyethylene glycol (PEG) spherical particles (Carbowax, Dow Chemical, Midland, MI, USA) at 200 MPa. The ratio between α-TCP powder and PEG particles was set at 0.70 g/g. To produce microporous samples (Mg and MG), wheat flour (Coop, Switzerland, www.coop.ch; d50 = 76 μm; bimodal distribution with peaks close to 30 μm and 100 μm) was added to these mixtures at a ratio of 1 g flour for 2 g PEG particles. Once isostatically pressed, various procedures were followed to achieve different microporosities and grain sizes: (i) mg samples: the samples were sintered 1 h at 1000 °C, cut into 12 x 12 x 45 mm prisms, and machined into Ø = 8 mm x L = 13 mm cylinders; (ii) Mg samples: the pressed samples were machined into Ø = 8.35 mm x L = 13.50 mm cylinders, and sintered 1 h at 1000 °C; (iii) mG samples: the pressed samples were machined into Ø = 8.31 mm x L = 13.45 mm cylinders, and sintered 1 h at 1300 °C followed by 24 h at 900 °C; (iv) MG samples: the pressed samples were machined into Ø = 8.60 mm x L = 13.65 mm cylinders, and sintered 1 h at 1300 °C followed by 24 h at 900 °C. Once all 4 sample types were prepared, all samples were cleaned in ethanol, and calcined 1 h at 900 ºC. As the mG samples still contained large amounts of α-TCP after this calcination step, these samples were calcined once again at 900 °C for 12 h. The samples were then inserted into 1.5 mL micro-centrifuge tubes (4182.1, Carl Roth, Karlsruhe, Germany), packaged once in a peel (Stericlin®) and sterilised by γ-irradiation with a 25 kGy dose (Synergy Health, Däniken, Switzerland).

Scaffold characterisation
Various methods were used to characterise the physical and chemical properties of the four tested scaffolds: size and weight measurements, specific surface area measurements (SSA), materialography, scanning electron microscopy (SEM), micro-computed tomography (μCT), Mercury (Hg) porosimetry, x-ray diffraction (XRD). More details are provided hereafter.

Geometrical density and porosity
To determine the geometrical density and porosity, three samples per group were measured with a caliper gauge and weighed. The geometrical density, also called apparent

density, was always reported to β-TCP theoretical density (3.07 g/cc) to calculate the relative density and infer the porosity.

Specific surface areas

The SSA values were determined by N_2 adsorption at 77 K (Gemini 2360, Micromeritics, Norcross, GA, USA) applying the Brunauer-Emmett-Teller (BET) model with 5 point determination. Three samples per group were dried several hours at 130 °C under constant N_2 flow.

XRD

The crystalline composition of the scaffolds was assessed by XRD using a powder diffractometer (X'Pert Pro MPD, PANalytical, Netherlands) with Ni-filtered CuKα radiation in the range from 5-60° 2θ. The quantitative phase composition was determined by Rietveld refinement using the software Fullprof.2k (http://www.ill.eu/sites/fullprof/) version 5.00 (Rodriguez-Carvajal, 2001). Structural models were taken from Mathew *et al*. (Mathew *et al.*, 1977) for α-TCP, from Schroeder *et al*. (Schroeder *et al.*, 1977) for β-TCP and from Sudarsanan *et al*. (Sudarsanan and Young, 1969) for hydroxyapatite (HA; $Ca_5(PO_4)_3$). No other phases were identified in the diffraction patterns.

Materialography

Materialography was used to determine porosity, micropore diameter, and grain size. For that purpose, three samples per group were embedded in a resin (EpoFix, Struers, Birmensdorf, Switzerland). The samples were then polished (final polishing step with a water free 0.2 μm silica suspension from Akasel) and observed by SEM using backscattered electrons. Image analysis was used to quantify the total porosity (number of pixels under and above an optically set threshold value of grey tones), the macroporosity (fraction of grid points falling on a macropore), and the porosity within the microporous regions. Additionally, the micropore size and the grain size distributions were estimated using a distance mapping/ fuzzy distance algorithm (Bashoor-Zadeh *et al.*, 2011). Centreline skeletons passing through the maxima of the distance maps of void and grain structures, respectively, were used to determine the average sizes. For each pixel of the skeleton, the maximum circle that could be inscribed locally to fit the structure was determined and its diameter was registered. This process was repeated for each pixel of the skeleton of the void and grain spaces, respectively, hence resulting into a size distribution. The average sizes of both the void and grain structures were calculated by averaging the diameter circles registered.

Scanning electron microscropy

SEM examinations were performed with an EVO MA25 microscope (Zeiss, Oberkochen, Germany). Prior to their examination, all samples were carbon coated twice.

Micro-computed tomography

μCT imaging was performed on a μCT 50 scanner (Scanco Medical, Brüttisellen, Switzerland). Scaffolds were scanned with an isotropic nominal resolution of 10 μm before *in vivo* implantation in a dry state (final cleaning and

sterilisation were performed after μCT scanning) and after implantation, in 70 % ethanol (explants comprising the scaffold and part of the surrounding bone). Energy was set to 55 kV, intensity to 145 μA, integration time was 200 ms and a 2-fold frame averaging was used. A constrained Gaussian filter was applied to the resulting images using a filter width of 0.8 and filter support of 1. Morphological parameters of the scaffolds before implantation were evaluated on a smaller cylinder with 4 mm diameter and 6.5 mm height from the middle of the scaffold to avoid influence of the surface. Threshold for segmentation was chosen individually per material and was 330 mg HA/ccm for Mg and 440 mg HA/ccm for mg, mG and MG. Scaffold volume density (BV/TV), macroporosity, connectivity density and pore size distribution was evaluated with the same analysis as used for human bone biopsy (Hildebrand *et al.*, 1999).

Samples after implantation were measured with the same settings. Some samples were damaged during operation procedure and excluded from the quantitative analysis. Images post-implantation were scaled to 20 μm resolution and orientated along the defect axis before Gaussian filtration. An iterative threshold algorithm was applied which automatically determined a threshold based on the histogram. Iterative thresholds varied for samples mg between 432 and 555 mg HA/cc, for samples Mg between 415 and 567 mg HA/cc, for samples mG between 441 and 535 mg HA/cc and for samples MG between 415 and 533 mg HA/cc. Three different regions of interests (ROI) were analysed per sample by applying cylindrical masks of different sizes. Cylinder diameter was kept to the original defect diameter of 8 mm, height varied between 2 mm, 4 mm and 6 mm. The mask was placed for all samples on the bottom of the drill hole at the location where the maximum bore was reached. BV/TV inside the cylinders was assessed, which represents remaining scaffold and newly formed bone (contrary to a past study (Von Doernberg *et al.*, 2006), in the present study it was not possible to distinguish bone from the scaffold).

Hg porosimetry

Hg porosimetry measurements were performed with a Pascal 140/440 porosimeter (Thermo Fisher Scientific, Reinach, Switzerland) with the aim to determine the size of open pores in the range between 7 nm and 100 μm using the Washburn equation. Surface tension and contact angle of mercury were set to 0.480 N/m and 140°, respectively and pressure was applied up to 200 MPa. Three samples from each group were dried overnight at 130 °C in order to drive off any adsorbed water from the sample. Multi-cycle porosimetry was performed to determine the neck size connected to the ink-bottle pores (pores that are connected to the outer part of the scaffold only through narrow pores) (Van Garderen *et al.*, 2012).

Implantation procedure

The animal experiments were conducted according the Swiss law of animal welfare and protection and were granted by the local authorities (Kantonales Veterinäramt: authorisation # 199/2010). Eighteen female 3-year old Swiss Alpine sheep (63-77 kg body weight (bw.)) served as

experimental animals. A well-established drill-hole model in sheep was used to study the effect of microporosity and grain size on resorption behaviour and new bone formation (Nuss *et al.*, 2006). Briefly, 8 mm drill holes in diameter and 14 mm in depth were drilled in the proximal and distal epiphyses of the humerus and femur. After flushing and cleansing the holes were filled randomly with the implants matching in size. Care was taken not to damage the edges of the ceramics during implantation. For this the implants were inserted through a drill guide of the same size held directly above the edges of the drill hole and gently pushing the implants with a flat insert into the drill hole. Eight materials were implanted per sheep, and 6 sheep were taken per implantation time (2, 4 and 8 weeks), leading to a total of 144 samples. Here, only the results of the four materials varying in microporosity and grain size are presented in details (4 materials x 3 time points x 6 repeats = 72 samples). This decision is supported by the fact that four of the eight calcium phosphate materials did not address the aim of the present study. Also, presenting the complete dataset would extend the study quite markedly without changing the conclusion.

All surgeries were performed under general inhalation anaesthesia, and after recovery the sheep were allowed to roam free in stalls under appropriate antibiotic and analgesia regimen (benzylpenicillin 35000 IE/kg bw.; gentamicin sulphate 4 mg/kg bw.; buprenorphine 0.001 mg/kg bw.; carprofen 4 mg/kg bw. for 3 days).

Implants were retrieved after slaughtering of the animals by cutting bone blocks containing the original size of the ceramics and a safety margin of minimally 4 mm at each side. The position of the original marker to indicate the location was respected and identified as good as possible before processing the samples for histology of non-decalcified bone blocks (Engelhardt and Gasser, 1995; Von Doernberg *et al.*, 2006). Briefly, bone samples were fixed in 40 % ethanol and then dehydrated in a series of ethanol solutions (40-100 %) before being defatted in xylene. Importantly, µCTs of all samples were performed in the middle of the dehydration process, when samples were fixed in 70 % ethanol. Infiltration with polymethylmethacrylate was done under vacuum at 4 °C and final polymerisation at room temperature. Ground sections were prepared using a precision saw (Leica SP 1600, Leica Microsystems, Nussloch, Germany) and cutting blocks transversely at a 90° angle to the insertion axis and at two levels (A and B). Sections were surface stained with toluidine blue. Toluidine blue selectively stains acidic tissue components (sulphates, carboxylates, and phosphate radicals), in particular polyanions (*e.g.*, cartilage matrix, bone) (Sridharan and Shankar, 2012). Additionally, two thin sections (5 µm) were cut with a Microtome (Leica RM2155, Leica Microsystems, Wetzlar, Germany), placed on a sample holder coated with chromium gelatin, covered with a Kisol foil, dried for two days at 42 °C, and finally stained with either van Kossa/ McNeal or toluidine blue. The latter sections were used to assess the cell response.

Evaluation of histological samples was conducted qualitatively and also quantitatively using for the latter a customised software program (Leica Quips/Qwin,

Leica Microsystems). Percentage of newly formed bone, remaining ceramic and granulation tissue was calculated by two independent reviewers, and results were compared between groups. This quantification was done in three concentric rings (outer ring, middle ring, inner ring) (Von Doernberg *et al.*, 2006). The cell response was assessed semi-quantitatively on the thin histological sections. For that purpose, cells were counted in four areas of the defect filled with the ceramic. The areas (zones 1 to 4) were spread equidistantly between the defect borders and the centre of the defect. Four groups were considered: (i) osteoclasts (defined arbitrarily here as multinucleated giant cells lying on a bone surface), (ii) multinucleated giant cells (defined arbitrarily here as multinucleated giant cells lying on a ceramic or sitting away from a surface), (iii) macrophages, and (iv) lymphocytes and plasma cells.

Statistics

Statistical analysis of the µCT and histology results was performed with PASW Statistics 18 (SPSS Inc., Chicago, IL, USA) using a univariate ANOVA and Bonferroni Post-Hoc test. The results were also analysed using a three-way factorial design of experiments (parameters: grain size, microporosity, implantation time). Significance was considered to occur for $p < 0.05$.

Results

Scaffold characterisation

Composition
The Rietveld refinement analysis of the XRD results revealed that three of the four scaffold types contained almost 100 % of β-TCP (Table 2). The group mG contained 16 % α-TCP despite an additional thermal treatment at 900 °C for 24 h. All materials were well crystallised as indicated by the very narrow diffraction peaks and the absence of broad and high baseline.

SEM
Great care was taken to characterise the scaffold architecture. Various methods were used including SEM, geometrical density, materialography, Hg porosimetry and µCT. The next paragraphs will describe the results obtained with these methods.

No clear architectural differences could be detected by SEM at the macro level (Fig. 1). The macropores were fairly spherical and in a similar size range, close to 0.1-0.3 mm. However, the space between the macropores appeared to be looser or more porous going from sample mg to samples mG, Mg and MG. At a higher enlargement, much larger differences could be seen (Fig. 2). For example, mg samples presented a much finer and denser microstructure than MG samples. In fact, grain size, pore size, and porosity seemed to increase in the order mg, Mg, mG and MG. Interestingly, the group with a low microporosity and small grains (mg) presented a heterogeneous microstructure: dense zones as large as 10 µm in size were surrounded by sub-µm-sized solid particles.

Table 2. Crystalline purity, porosity, macroporosity ("MPor"; pores larger than 50 µm), and microporosity ("µPor") of the four scaffold types used in the animal study as determined by Rietveld refinement of XRD data, weighing, Materialography, Hg Porosimetry, and µCT. The results are reported as "mean ± one standard deviation".

Scaffold	XRD purity [%]	Weighing Porosity [%]	Materialography Porosity [%]	MPor [%]	µPor [%]	Hg Porosimetry Porosity [%]	MPor [%]	µPor[4] [%]	µCT Porosity [%]	MPor [%]	µPor [%]
mg	99 ± 1	78.3 ± 0.4	75 ± 4	65 ± 5	21 ± 3[1] 10 ± 9[2]	75.0 ± 1.0 72.0 ± 1.4[3]	11 ± 3	64 ± 4	56 ± 1	54 ± 2	2.5 ± 0.5
Mg	100 ± 1	83.8 ± 0.5	83 ± 1	61 ± 4	42 ± 11[1] 22 ± 5[2]	82.8 ± 0.7 76.4 ± 0.7[3]	22 ± 10	61 ± 11	58 ± 2	50 ± 3	7.6 ± 0.4
mG	84 ± 1[5]	78.6 ± 0.5	75 ± 3	65 ± 4	26 ± 1[1] 10 ± 7[2]	76.5 ± 0.1 73.8 ± 0.5[3]	47 ± 3	30 ± 3	59 ± 1	56 ± 2	3.1 ± 0.1
MG	100 ± 1	81.2 ± 0.7	78 ± 1	48 ± 7	56 ± 5[1] 30 ± 8[2]	77.9 ± 0.2 69.7 ± 2.6[3]	46 ± 1	32 ± 1	57 ± 3	50 ± 3	7.1 ± 0.2

[1]Porosity in the microporous regions; [2]Difference between porosity and macroporosity; [3]Ink-bottle porosity; [4] Difference between porosity and macroporosity: [5]The remaining 16 % consist of α-TCP.
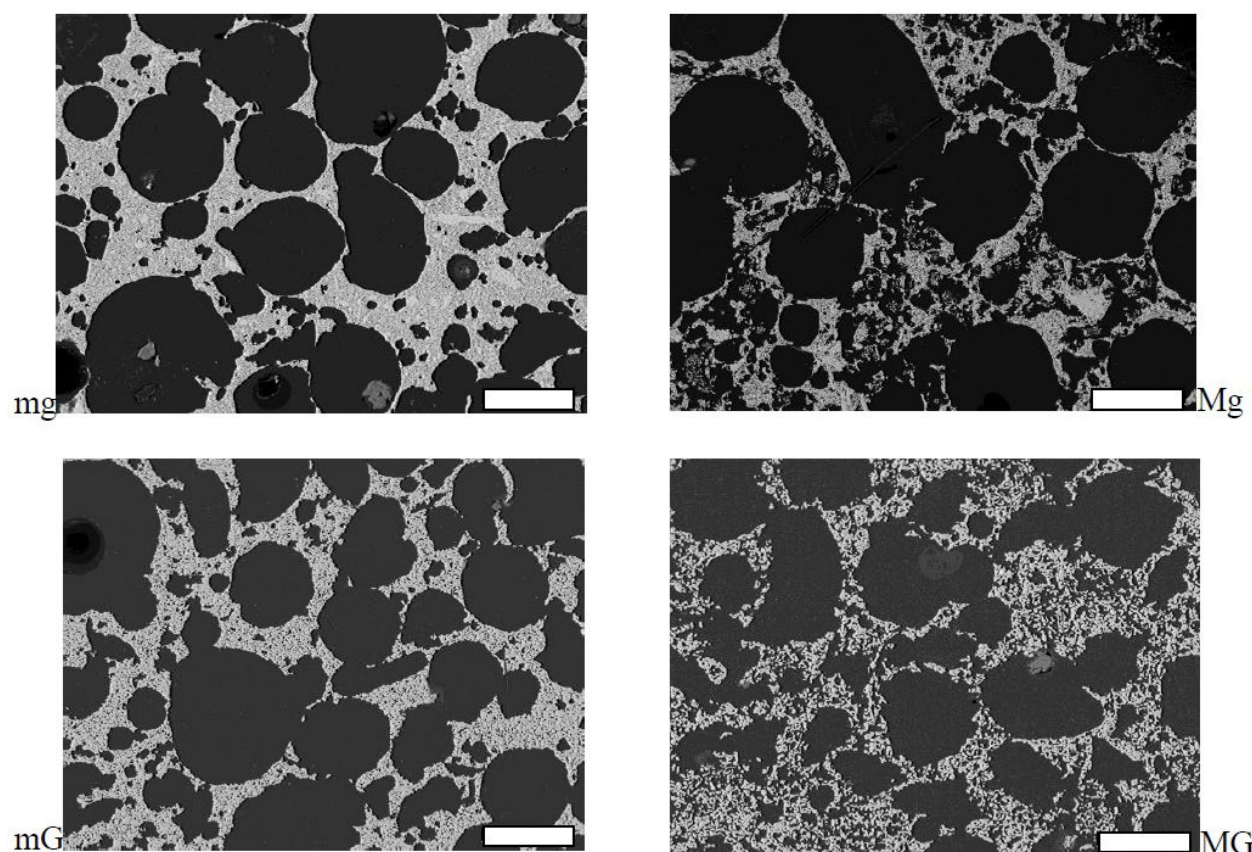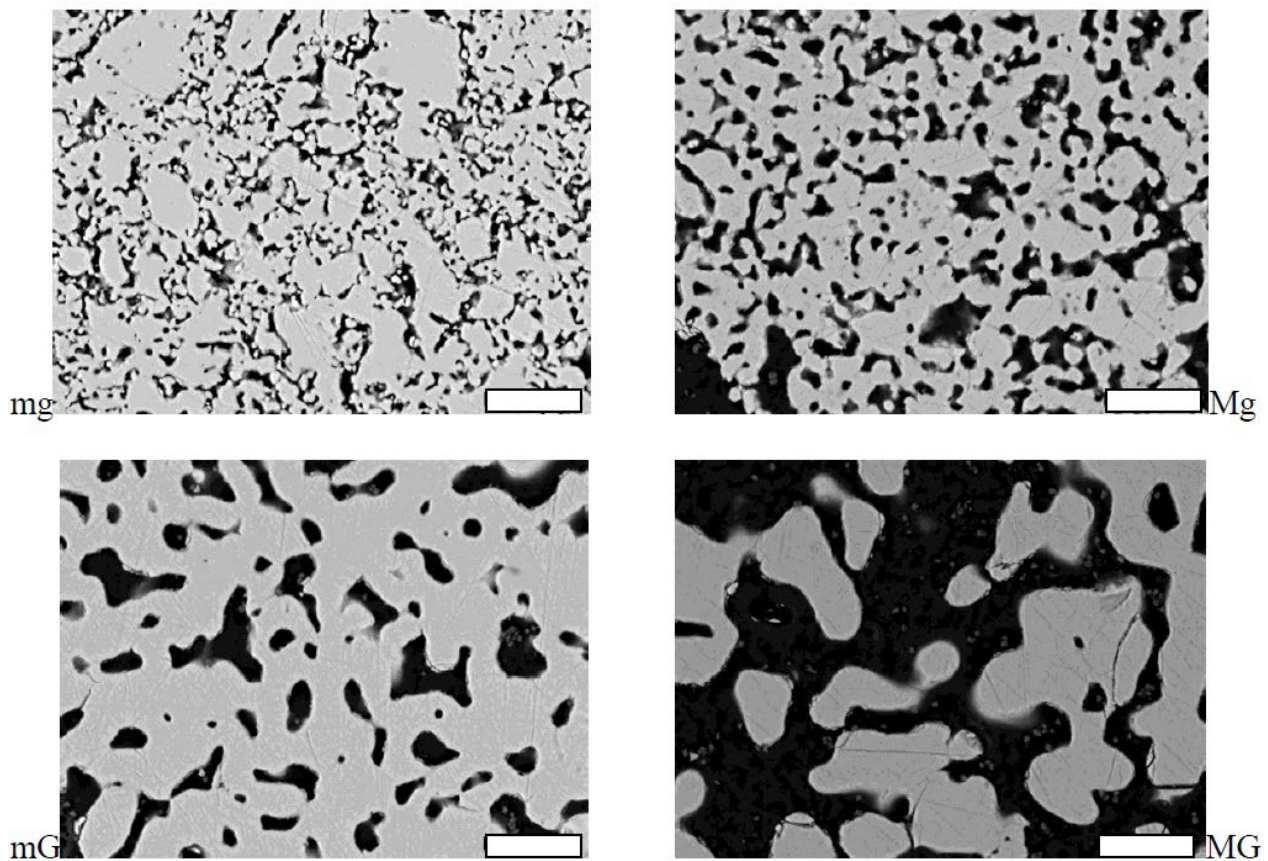

Fig. 1. SEM microstructures of the 4 tested materials: (mg) small microporosity, small grains; (Mg) large microporosity, small grains; (mG) small microporosity, large grains; (MG) large microporosity, large grains. The scale bar corresponds to 200 µm. The pores are black and the material is white.

Geometrical density
According to the geometrical density results obtained, by weighing and size determination, the porosity did not vary much between the different scaffold types (Table 2). The values ranged between 78.3 ± 0.4 % and 83.8 ± 0.5 %. Significantly, higher values were found for the two microporous samples (83.8 ± 0.5 % and 81.2 ± 0.7 %, against 78.3 ± 0.4 % and 78.6 ± 0.5 %).

Materialography
The porosities measured by materialography were roughly 3 % lower than those measured by weighing but were

consistent with them (Table 2). Whereas the porosities varied within a relatively short range (75 ± 4 % to 83 ± 1 %), larger changes were seen among macroporosities (from 48 ± 7 % to 65 ± 5 %) and microporosities (from 10 ± 9 % (mg) to 30 ± 8 % (MG)). The difference was even larger when looking at the porosities within the microporous regions. Here, the values varied between 21 ± 3 % (mg) and 56 ± 5 % (MG).

Image analysis allowed the determination of the micropore size and grain size (Table 3; Fig. 3; Fig. 4). The micropore size varied significantly between all samples, going from mean values of 0.47 ± 0.02 µm

Fig. 2. SEM microstructures of the 4 tested materials: (mg) small microporosity, small grains; (Mg) large microporosity, small grains; (mG) small microporosity, large grains; (MG) large microporosity, large grains. The scale bar corresponds to 10 μm. The pores are black and the material is white.

Table 3. Mean micropore diameter ("Mean μPor Ø"), mean grain diameter, mean pore diameter, and specific surface area (SSA) of the four scaffold types used in the animal study as determined by XRD, Materialography, Hg Porosimetry, μCT, and N_2 adsorption. The results are reported as "mean ± one standard deviation". The mean micropore size determined by materialography was based on representative images of microporous areas. It is the volume-based mean value.

Scaffold	Materialography		Hg Porosimetry	μCT		N_2 adsorption
	Mean μPor Ø[1)] [μm]	Mean grain Ø[1)] [μm]	Mean pore Ø[2,3)] [μm]	Mean pore Ø[3)] [μm]	Connectivity [mm⁻³]	SSA [m²/g]
mg	0.47 ± 0.02	1.27 ± 0.09	2.8 ± 1.0	169 ± 10	406 ± 94	0.79 ± 0.08
Mg	0.89 ± 0.11	1.29 ± 0.04	6.4 ± 3.7	153 ± 3	880 ± 29	0.64 ± 0.03
mG	1.44 ± 0.10	3.11 ± 0.05	15.7 ± 9.9	156 ± 3	520 ± 9	0.61 ± 0.02
MG	3.24 ± 0.09	3.43 ± 0.32	8.3 ± 1.5	122 ± 2	935 ± 45	0.37 ± 0.02

[1)]Number-based.

[2)]This value was calculated by considering that the pores were cylindrical (mean pore = 4 x pore volume / pore surface area).

[3)]Volume-based.

(mg) to 3.24 ± 0.09 μm (MG). These differences can be clearly identified on the cumulative pore size distributions (fraction of the pores smaller than a given value; Fig 4a). The two "large grain" groups (mG and MG) had significantly larger grain sizes (3.11 ± 0.05 μm and 3.43 ± 0.32 μm, respectively) than the two "small grain groups (1.27 ± 0.09 μm for mg and 1.29 ± 0.04 μm for Mg; Table 3; Fig 3; Fig. 4). However, no significant difference was noticed within the "large grain" and the "small grain"

groups. This similarity can be better assessed on the grain size distribution curves (Fig. 3b; Fig. 4b).
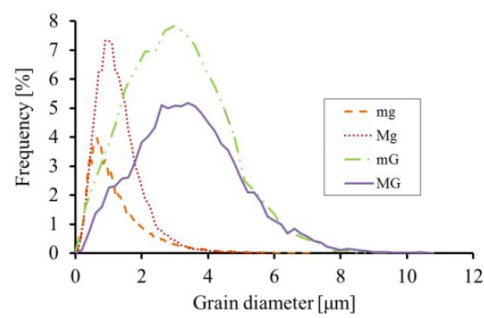
Hg porosimetry

The porosities determined by Hg porosimetry were very similar to those measured by weighing and materialography. The values ranged between 75.0 ± 0.1 % and 82.8 ± 0.7 % (Table 2). A large fraction of the pores consisted of pores smaller than 50 μm (= micropores). For example, sample
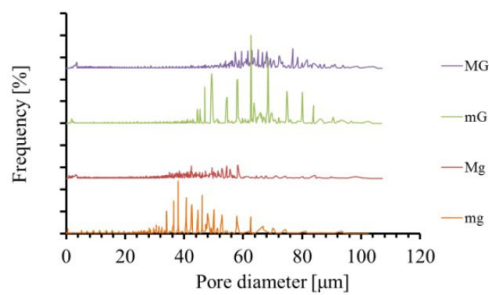
(a) Materialography
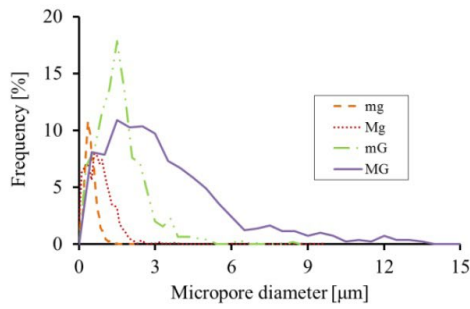
(b) Materialography

(c) Hg Porosimetry

(d) μCT

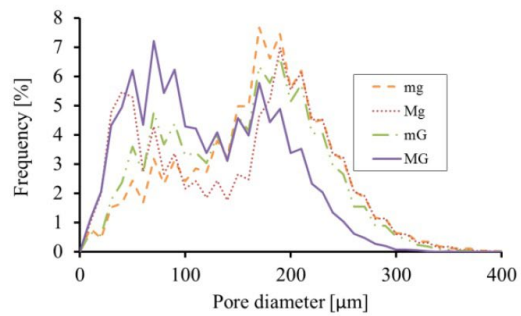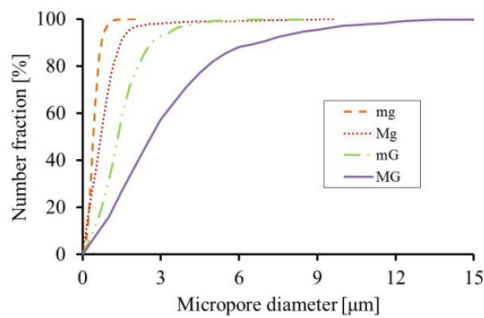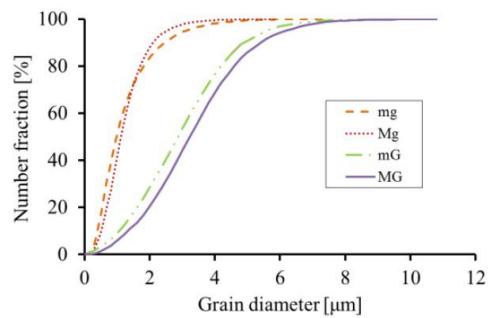**Fig. 3**. (**a**) Micropore size distribution (in number) as measured by image analysis of materialography images; (**b**) Grain size distribution (in number) as measured by image analysis of materialography images; (**c**) Pore size distribution (in volume) as measured by Hg porosimetry; (**d**) Pore size distribution (in volume) as measured by μCT. The total surface below the curves shown in (**a**), (**b**) and (**c**) is not constant because the number of intervals considered for each curve varies. For example, the mg and mG grain size curves contained 147 and 37 data points, respectively.
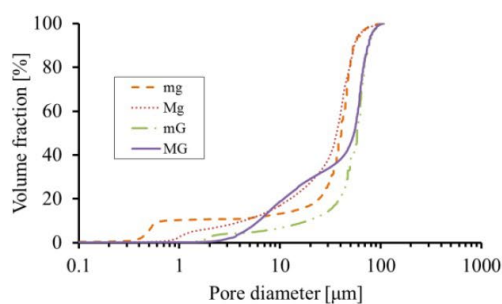
(a) Materialography

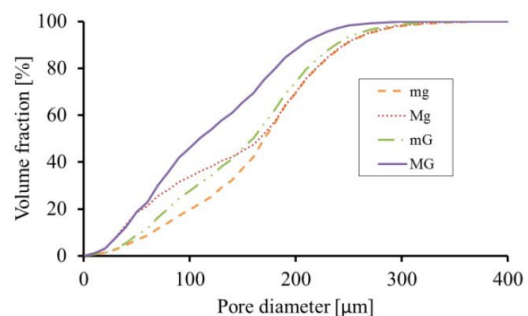(b) Materialography

(c) Hg Porosimetry

(d) μCT

Fig. 4. (**a**) Cumulative micropore size distribution as measured by image analysis of materialography images; (**b**) Cumulative grain size distribution as measured by image analysis of materialography images; (**c**) Cumulative pore size distribution as measured by Hg porosimetry; (**d**) Cumulative pore size distribution as measured by μCT.
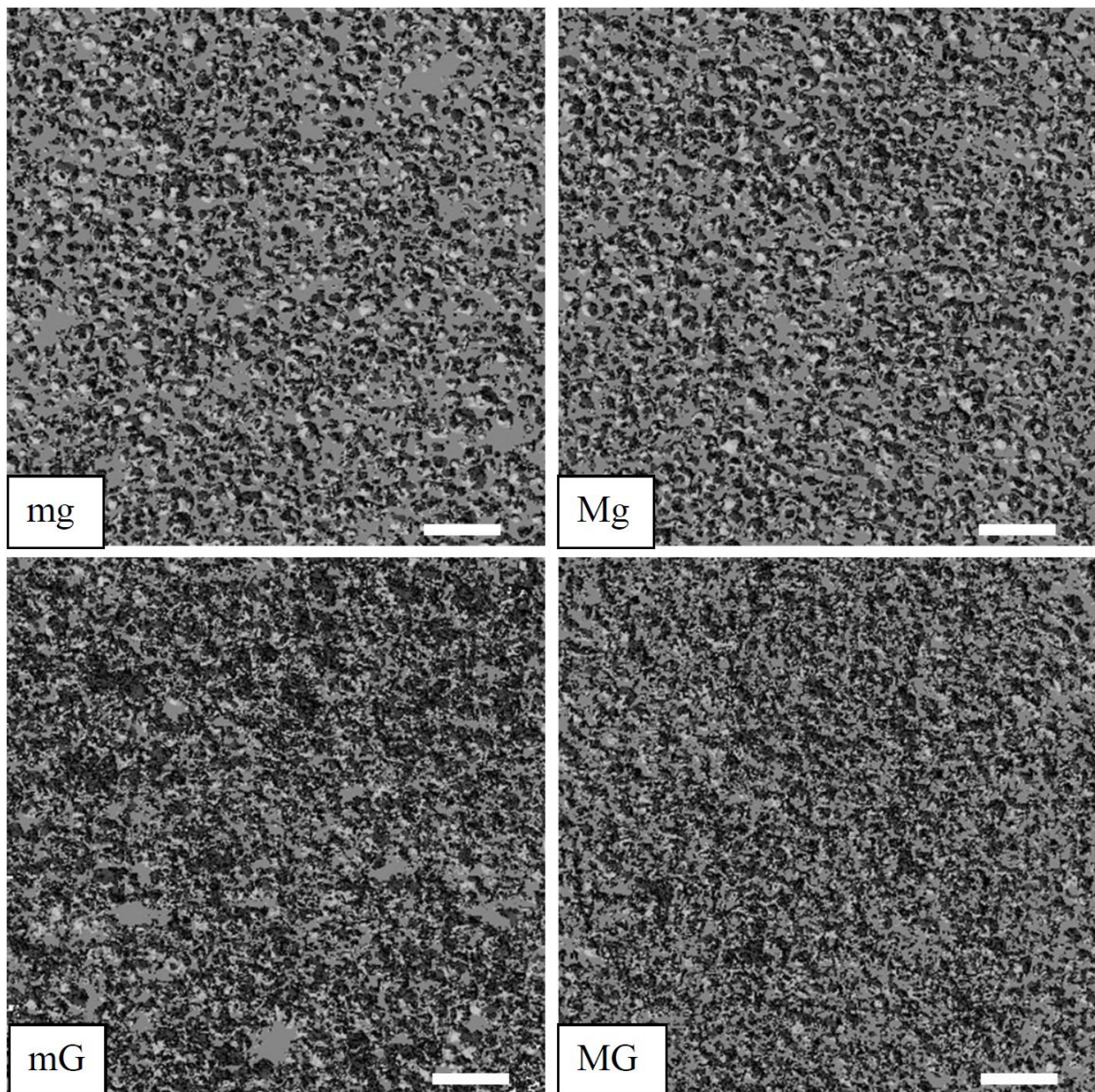
Fig. 5. Cross-sectional view of representative scaffolds before implantation imaged with µCT. The four groups are: (mg) small microporosity, small grains, (Mg) large microporosity, small grains, (mG) small microporosity, large grains, (MG) large microporosity, large grains. Scale bar is 1 mm.

Mg contained 61 ± 11 % microporosity (total porosity: 82.8 ± 0.7 %). However, a thorough analysis of the pore size distribution using a multicycle analysis revealed that most of the porosity consisted of ink-bottle porosity, *i.e.*, pores connected to the outer part of the scaffold by thin pores/necks. Once filled with Hg, these pores could not be emptied during depressurisation. Quantitatively, the difference between "porosity" and "ink-bottle porosity" varied between $76.5-73.8 = 2.7$ % (sample mG) and $77.9-69.7 = 8.2$ % (sample MG) (see Table 2).

The Hg porosimetry results also revealed clear differences of pore size distributions between the different groups. The two groups with large grains (groups mG and MG) contained bigger pores than those with small grains (groups mg and Mg; Table 2; Fig. 3c; Fig. 4c). This difference was particularly clear when looking at the diameter corresponding to a 50 % volume fraction (Fig. 4c). Interestingly, the two samples containing flour (Mg and MG) had the highest volume fraction of pores smaller than 20 µm (Fig. 4c).

µCT *results prior to implantation*
Scaffolds were scanned and evaluated regarding morphological parameters by means of µCT before implantation. The scaffold structure was clearly different between high (Mg and MG) and low (mg and mG) microporosity, with a stable round pore shape and more material between the pores for the low microporosity samples (Fig. 5). The influence of grain size was not visible on the µCT cross-sectional images.

Quantitatively, the porosity values measured by µCT were much lower than those measured by weighing and
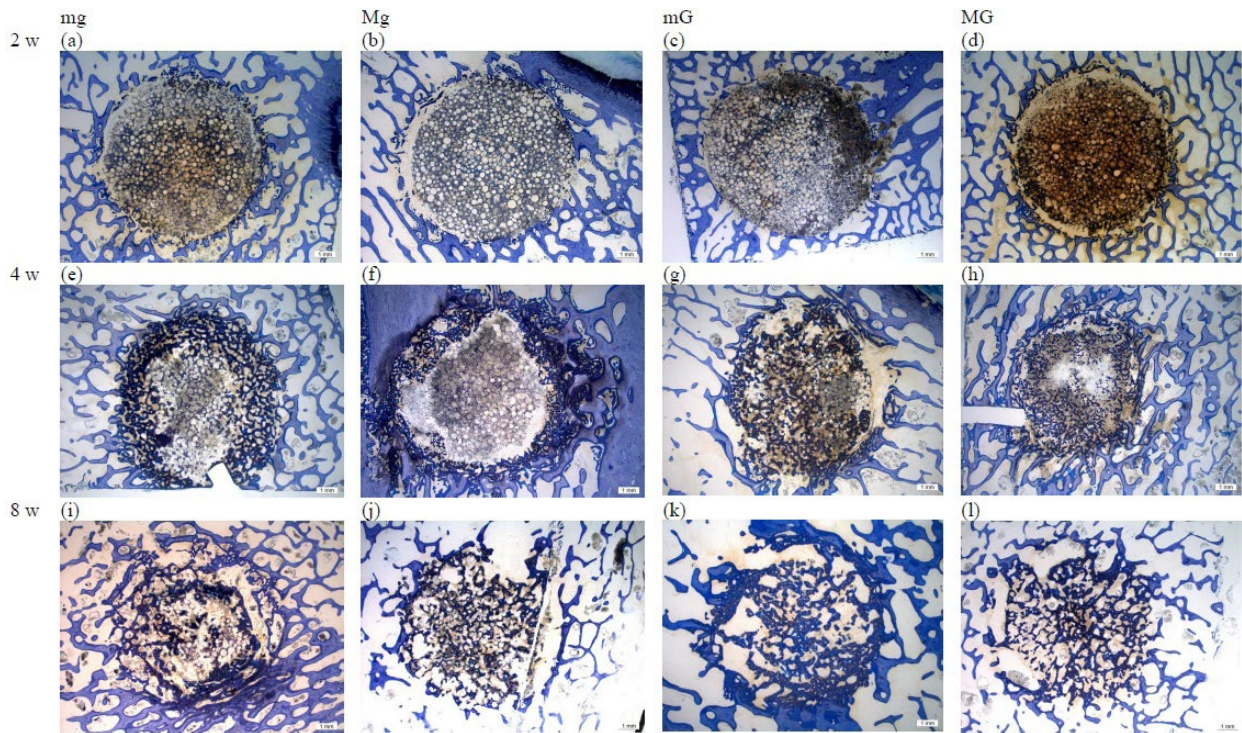
Fig. 6. representative histological (grinding) sections of the 4 tested materials at the three implantation times (2, 4 and 8 weeks). The scale bars correspond to a size of 1 mm.
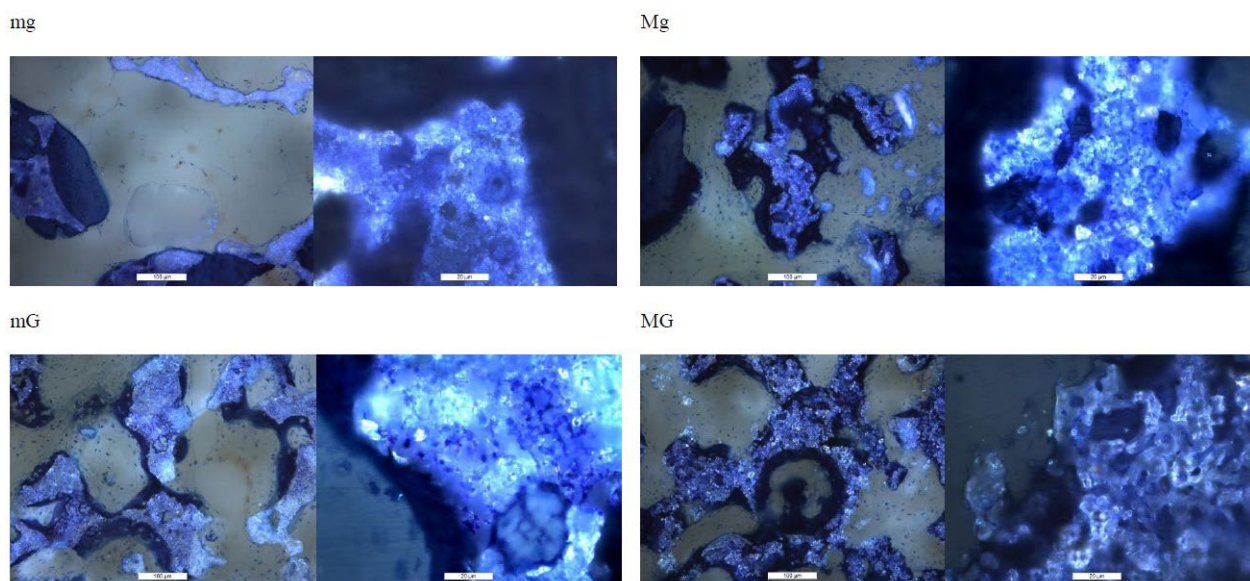

Fig. 7. representative histological (grinding) sections of the 4 tested materials showing the interdigitation between bone and ceramic. The sections are stained with toluidine blue. Bone appears in blue whereas the ceramic is whitish / translucent. For each material, two images are shown, one with a moderate enlargement (200 x; scale bar: 100 μm; left image) and one with a higher enlargement (1000 x; scale bar: 20 μm; right image).

materialography: instead of being close to 80 %, the values were slightly below 60 % (56 ± 1 % to 59 ± 1 %; Table 2). Most of the porosity resulted from the presence of pores larger than 50 μm. As a result, the microporosity (pores smaller than 50 μm) determined by μCT remained low (from 2.5 % ± 0.5 % (mg) to 7.6 ± 0.4 % (Mg)). Even though the microporosity values determined by μCT were much lower than those measured by materialography, they showed the same trend: samples supposed to have a high

microporosity (Mg: 7.6 ± 0.4 %; MG: 7.1 ± 0.2 %) were significantly more microporous than samples supposed to have a low microporosity (mg: 2.5 ± 0.5 %; mG: 3.1 ± 0.1 %).

All pore size distributions presented two peaks, one below 100 μm and the second one close to 200 μm, slightly shifted depending on the material (Fig. 3d). The latter peak was the largest for all samples but MG. On the cumulative plot (Fig. 4d), the curve for MG sample was markedly
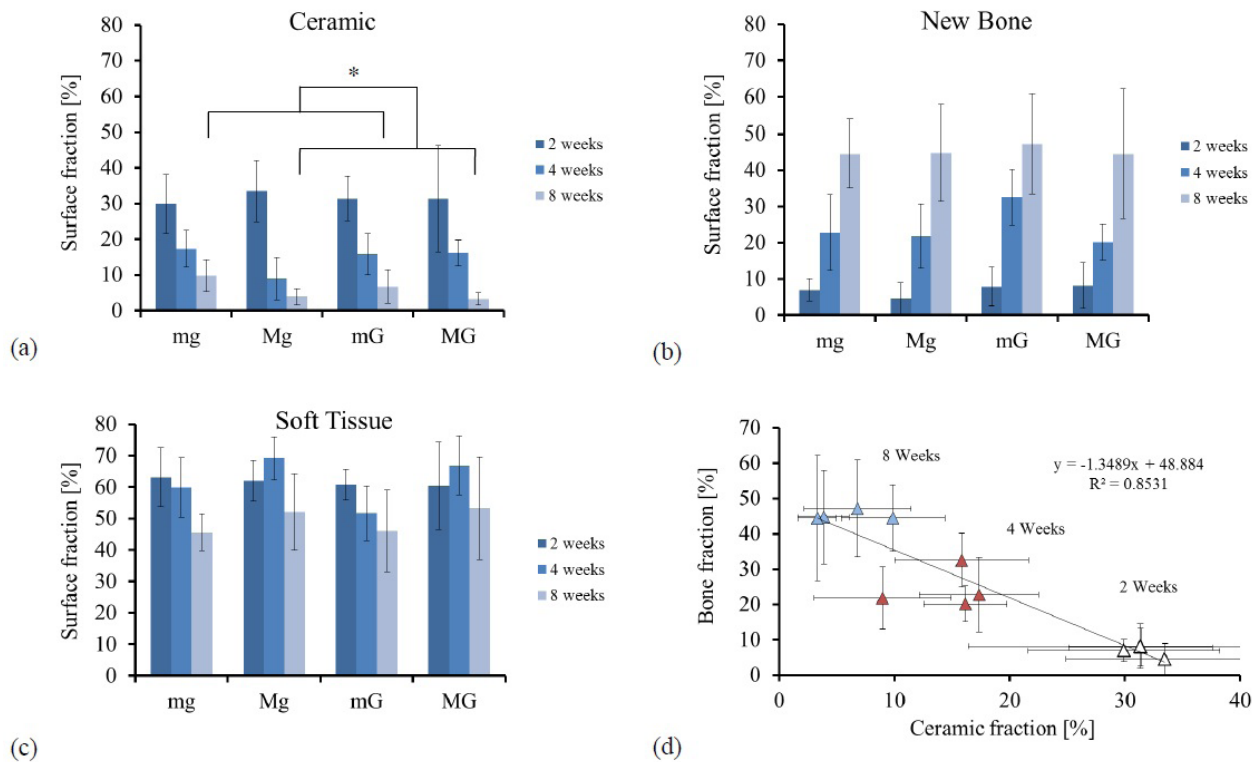
Fig. 8. Histomorphometrical evolution of (**a**) ceramic, (**b**) bone and (**c**) soft tissue content upon implantation for the 4 implanted ceramics. Correlation between ceramic and bone fraction (**d**). The three different symbol colours are used to distinguish the three different implantation times (blue: 8 weeks; red: 4 weeks; white: 2 weeks). The ceramic fraction of highly microporous samples was significantly lower at 4 and 8 weeks implantation than that of samples with lower microporosity (Fig 7a; "*").
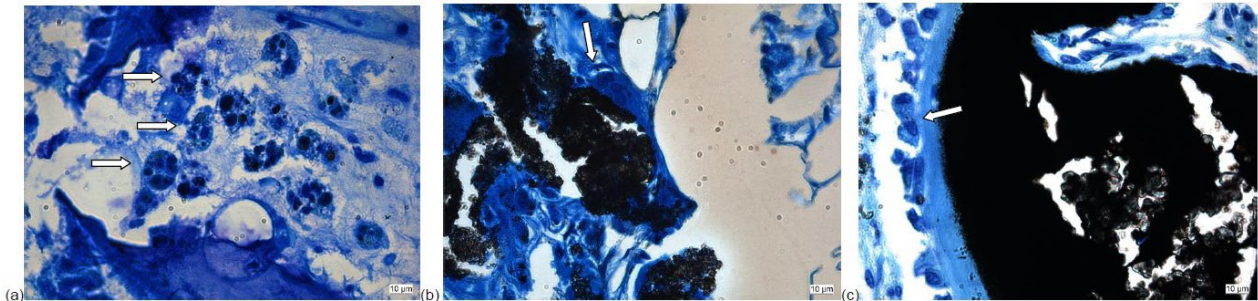

Fig. 9. Representative histological observations at the cellular level: (**a**) macrophages filled with ceramic residues (three macrophages are shown with an arrow); (**b**) multinucleated giant cell (arrow) sitting on a piece of ceramic (black colour); (**c**) osteoblast layer along an osteoid tissue sitting on a piece of ceramic.

higher than all other curves. This was mainly due to a steep increase of the curve up to a pore diameter of 100 μm.

The density of pore interconnections was expressed by the mean connectivity density (Table 3). This value varied between 406 ± 94 mm^{-3} for mg group and 935 ± 45 mm^{-3} for MG group. Whereas the effect of grain size was moderate ($+ 85$ mm^{-3} on average between small and large grain size groups), the effect of microporosity was extensive ($+ 445$ mm^{-3} on average).

SSA values

The SSA values were significantly higher for the two groups with the smallest grain sizes: 0.79 ± 0.08 m^2/g and 0.64 ± 0.03 m^2/g for mg and Mg group respectively, against 0.61 ± 0.02 m^2/g and 0.37 ± 0.02 m^2/g for mG and MG groups, respectively (Table 3). Whereas the latter result was expected, the significant decrease of the SSA values with an increase of microporosity was unexpected. The decrease was -0.13 m^2/g and -0.24 m^2/g for small and large grains, respectively.

Animal experiments

Implantation of ceramic scaffolds went well and all animals recovered without problems from surgery. No postoperative complications occurred and all specimens could be harvested after sacrifice of the animals. However, problems were encountered to locate the samples after implantation so several samples were damaged (cut) during

the retrieval procedure (*e.g.*, Fig. 6e, Fig. 6h, Fig. 6j). Also, toluidine blue did not stain all sections homogeneously (*e.g.*, Fig. 6h), rendering image analysis difficult.

Qualitative evaluation of histology sections did not reveal major differences between the four scaffold types (Figs. 6 and 7). In all samples, ceramic resorption and bone replacement occurred from the periphery to the centre (Fig. 6). Generally, new bone was found in the outer regions of the early specimens (2 weeks) and granulation tissue in the inner regions, whereas already at 4 weeks small mineralisation nests and at 8 weeks new bone were found also within the inner regions. Overall, the picture was similar in all scaffold types with only few differences between them. At 8 weeks all groups showed trabecular bone and few remaining scaffold material, although it appeared that the mg group showed the densest and most regular trabecular bone structure compared to the other three groups. Also, low microporosity samples (mg and mG groups) seemed to show a more intact structure at the early time point of 2 weeks compared to those with a high microporosity. On the other hand, no obvious effect of grain size was noticed. In all four scaffold types, a tissue stained in blue was found within the microporous regions (Fig. 7). This blue stained tissue is called "bone" further in this document.

Problems occurred with the quantitative evaluation especially in the early specimens (2 weeks). Since bone often formed within the ceramic micropores it was not possible to distinguish by computer technology the various fractions of new bone and remaining scaffold material (Fig 7). Therefore, semi-quantitative evaluation was also performed where the eye of the observers could more easily distinguish between the various fractions.

The ceramic fraction decreased whereas the bone fraction increased from 2 to 8 weeks implantation (Fig. 8a, b). Since the two processes occurred almost simultaneously and to the same extent, the soft tissue fraction remained fairly constant throughout the whole implantation period (Fig. 8c) and a negative correlation was found between ceramic and bone fraction (Fig. 8d). Among all results, there were only two significant effects: the ceramic fraction of highly microporous samples was significantly lower at 4 and 8 weeks implantation than that of samples with lower microporosity ($p < 0.01$). Simultaneously, there was more soft tissue in highly microporous samples ($p < 0.01$). In other words, the qualitatively superior behaviour of mg and to a smaller extent mG was supported statistically by histomorphometry.

Some variations were observed between sheep at all time-points. For example, the mean ceramic fraction measured in one sheep varied in the range of 27-43 % at 2 weeks, 19-29 % at 4 weeks, and 6-18 % at 8 weeks. Smaller differences were observed for the bone fraction: 4-8 % at 2 weeks, 17-25 % at 4 weeks, and 35-44 % at 8 weeks. To increase the sensitivity of our analysis, results within a sheep were normalised relative to the mean, and the statistical analysis was performed again. However, the conclusions were the same as those without normalisation.

No statistical difference of the cell response was found between the four scaffold types (Table 4). Generally, the number of cells varied radially from the outer zone (Z1)
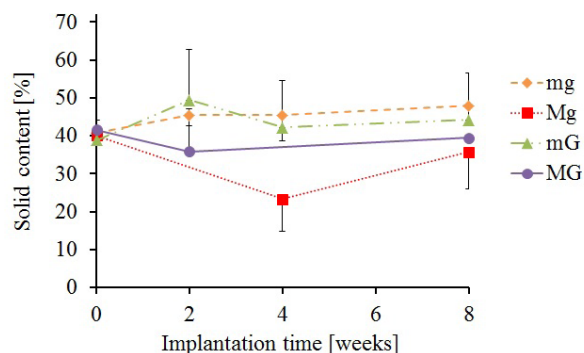

Fig. 10. Solid content as a function of implantation time. The values at time zero represent the solid content (= (bone + ceramic)/total volume) of the scaffold before implantation. $n = 18$ for data at time point 0 and $n = 4$ - 6 for data at 2, 4 and 8 weeks, depending on the amount of missing samples. In two conditions (Mg, 2 weeks and MG, 4 weeks), two many samples were missing.
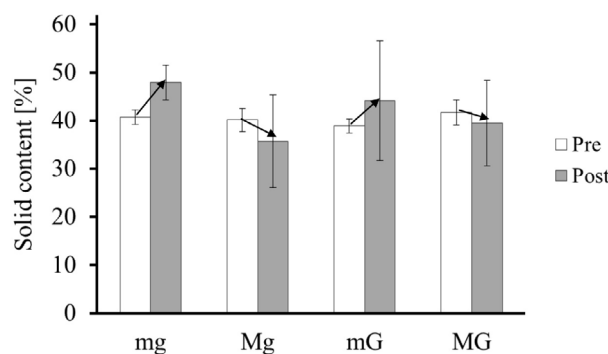

Fig. 11. Comparison of solid content ((bone + ceramic)/ total volume) before implantation and after 8 weeks implantation *in vivo* (dark colour) for the four tested scaffold types. The post-implantation results were evaluated with a 6 mm mask. The evolution of the solid content was significantly different when comparing samples with low and high microporosity (see the directions of the arrows for mg and Mg on one side, and Mg and MG on the other side).

to the inner zone (Z4) over time. So, at early time, most cells were found in the outer zone. At later time points, most cells were found in the central area. The ceramic was partly resorbed by macrophages and multinucleated giant cells (Fig. 9).

µCT *results post implantation*
Parallel to the histomorphometry results, the *in vivo* samples were also analysed by µCT to evaluate quantitatively the evolution of ceramic and bone content after implantation. Regions of interest (ROIs) of different sizes were defined with masks and applied always at the same location of a sample. Since no significant difference was seen by choosing the 2, 4 or 6 mm mask, only the 6 mm mask results are presented. The solid content (bone + scaffold volume fraction) of the four material groups is shown in Fig. 10 according to the evaluated ROI and implantation
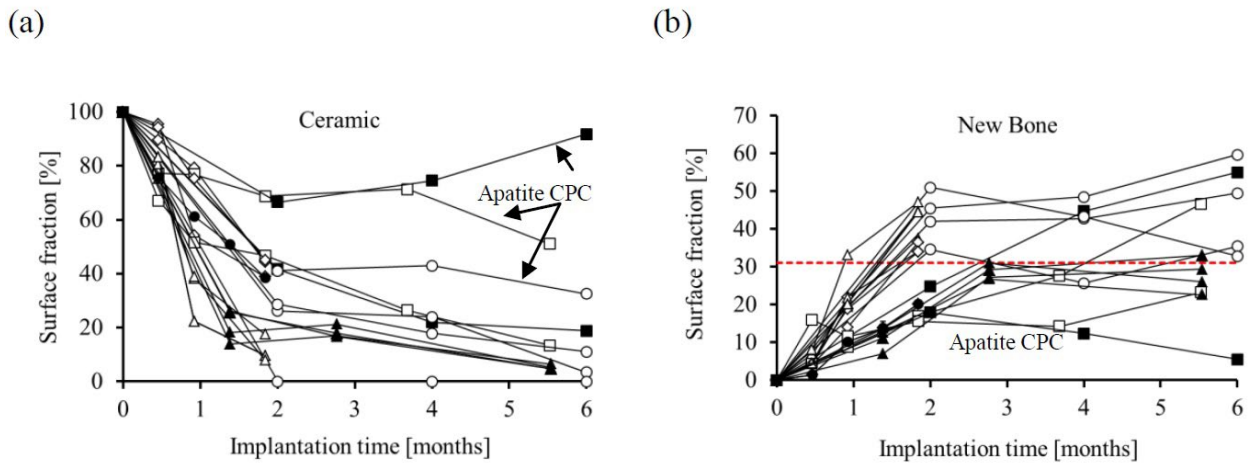
(a)

(b)

Fig. 12. Histomorphometrical results obtained in different studies by the same team and with the same sheep model (Nuss *et al.*, 2006). Two results are reported: (**a**) ceramic content, and (**b**) bone content. The bone graft substitutes had various compositions (β-TCP, brushite, monetite, apatite, gypsum) and forms (scaffolds, cements). The various symbols were used: (Δ) Results of the present study with β-TCP scaffolds; (▲) β-TCP scaffolds varying in macropore size between 150 and 1200 μm (von Doernberg *et al.*, 2006). (o) Results with four cements: gypsum, brushite without and with additional β-TCP granules, and apatite cement (= apatite CPC) (von Rechenberg *et al.*, 2013). (●) Brushite cement (Theiss *et al.*, 2005). (□) Brushite and apatite cement (Oberle *et al.*, 2005). (■) Brushite and apatite cement (Apelt *et al.*, 2004); (◊) β-TCP and monetite (unpublished results). For clarity reasons, no standard deviations were added. The dashed horizontal line corresponds to the mean fraction of bone that can be expected in a healthy animal.

time. Even though differences between groups were not significant, the highly microporous samples had the lowest solid content.

The solid content before implantation was compared with the solid content (scaffold + bone) after 8 weeks *in vivo* (Fig. 11). Univariate ANOVA did not show any statistically significant influence of time, but a significant influence of the material as well as time and material combined: whereas the solid content increased during implantation for samples with low microporosity (mg and mG), the opposite was found for highly microporous samples.

Discussion

Design

The aim of this study was to decipher the link between grain size, microporosity, and *in vivo* behaviour of β-TCP scaffolds. For that purpose, an attempt was made to design scaffolds according to a factorial design of experiments where the two investigated factors would be microporosity (low ↔ "m"/high ↔ "M") and grain size (small ↔ "g", large ↔ "G"). Ideally, the samples were meant to only vary according to these two parameters, *i.e.* both the total porosity and the mean macropore size were meant to be kept constant. To control the architecture, the idea was to play with two parameters affecting ceramic sintering: time and temperature. It is indeed known that ceramic densification and grain growth are two distinct phenomena (Chen and Chen, 1996; Chen and Chen, 1997; Chen and Wang, 2000). Whereas grain growth is favoured at high temperature, densification is mostly a function of the

ceramic density and grain size. Therefore, full densification can be achieved by two-step sintering: in a first stage, the ceramic is heated up at high temperature to rapidly reach a density superior to ≈ 75 %, and then the temperature is reduced by a few hundred degrees to fully densify the ceramic without concomitant grain growth (Chen and Wang, 2000). For example, Mazaheri *et al*. sintered 98 % dense hydroxyapatite 60 s at 900 °C and 2 h at 800 °C and were able to reduce the grain size from 1.7 μm to 190 nm (Mazaheri *et al.*, 2009).

In the present study, numerous samples were synthesised to achieve the required compositions and architectures. Specifically, samples were prepared by one and two-step sintering, at heating rates ranging from 1 to 5 °C/min, with dwell times ranging from 1 to 15 h, and with plateau values ranging from 600 to 1300 °C. During two-step sintering, the first plateau was either the highest in temperature to achieve high densification, or the lowest to achieve poor densification. The temperature of the second plateau was then selected to either coarsen the grains or keep the grains small. Results showed that it was not possible to play much with the two-step sintering (data not shown), perhaps because a high densification could not be achieved. Therefore, it was decided to add a fine combustible additive (wheat flour) into the α-TCP, PEG and stearic acid mixtures to create additional micropores. The success was limited because the wheat flour particles were fairly large, with peaks in the volume distribution close to 30 μm and 100 μm. Also, it appeared that a change of microstructure affected the ability of α-TCP raw material to convert to β-TCP during sintering. Specifically, mG samples contained 16 % α-TCP despite the fact that these samples were submitted to an additional thermal treatment

Table 4. Summary of the semi-quantitative cell response. Four groups were considered: (i) osteoclasts (defined arbitrarily here as multinucleated giant cells lying on a bone surface), (ii) multinucleated giant cells (MNGC; defined arbitrarily here as multinucleated giant cells lying on a ceramic or sitting away from a surface), (iii) macrophages, and (iv) lymphocytes and plasma cells (LP&P). Four zones were considered from the periphery (Z1) to the core (Z4).

Cell	Zone	2 weeks				4 weeks				8 weeks			
		mg	Mg	mG	MG	mg	Mg	mG	MG	mg	Mg	mG	MG
Osteoclasts	Z1	5.7 ± 2.7	5.8 ± 3.0	3.2 ± 1.9	2.8 ± 1.0	2.0 ± 1.3	3.0 ± 2.8	4.3 ± 4.1	4.8 ± 5.0	2.2 ± 0.4	3.0 ± 1.3	3.2 ± 1.7	2.0 ± 0.9
	Z2	1.8 ± 1.7	1.4 ± 1.5	1.2 ± 1.2	0.5 ± 0.8	4.7 ± 4.0	3.6 ± 2.5	3.2 ± 1.6	1.8 ± 1.0	3.4 ± 1.7	2.7 ± 1.0	3.3 ± 1.5	2.5 ± 1.0
	Z3	0.3 ± 0.8	0.0 ± 0.0	0.0 ± 0.0	0.2 ± 0.4	1.8 ± 1.0	2.0 ± 1.8	2.0 ± 1.1	2.5 ± 2.1	3.0 ± 0.7	2.2 ± 1.2	3.2 ± 3.1	2.2 ± 1.5
	Z4	0.2 ± 0.4	0.0 ± 0.0	0.0 ± 0.0	0.0 ± 0.0	0.7 ± 1.6	1.4 ± 2.1	1.2 ± 1.5	0.8 ± 1.0	3.2 ± 0.8	2.8 ± 1.8	2.3 ± 2.6	2.5 ± 2.1
MNGC	Z1	4.7 ± 3.4	3.8 ± 4.6	1.8 ± 2.2	3.0 ± 3.1	1.5 ± 1.4	0.8 ± 1.3	0.8 ± 0.4	2.8 ± 3.4	0.2 ± 0.4	0.0 ± 0.0	0.0 ± 0.0	0.0 ± 0.0
	Z2	5.7 ± 3.4	7.8 ± 5.2	2.2 ± 1.5	5.0 ± 4.7	6.7 ± 7.4	3.4 ± 4.5	4.7 ± 5.9	5.0 ± 5.3	0.0 ± 0.0	0.8 ± 1.6	0.0 ± 0.0	0.0 ± 0.0
	Z3	3.5 ± 1.6	4.8 ± 2.6	1.7 ± 2.4	1.5 ± 1.2	4.5 ± 4.0	5.4 ± 4.4	2.5 ± 3.1	8.3 ± 5.6	0.2 ± 0.4	1.2 ± 2.0	0.8 ± 1.3	0.2 ± 0.4
	Z4	3.3 ± 3.5	3.4 ± 2.1	0.7 ± 0.8	2.5 ± 3.8	3.8 ± 5.1	7.2 ± 7.3	1.7 ± 1.4	13.3 ± 12.0	0.2 ± 0.4	1.3 ± 2.3	0.7 ± 0.8	0.2 ± 0.4
Macrophages	Z1	5.8 ± 3.4	9.0 ± 5.3	4.2 ± 0.8	8.0 ± 4.4	6.2 ± 3.3	3.6 ± 2.7	4.2 ± 3.3	5.0 ± 2.1	0.4 ± 0.5	0.3 ± 0.8	0.8 ± 0.8	1.2 ± 1.8
	Z2	6.7 ± 8.5	9.6 ± 10.4	6.2 ± 2.0	4.5 ± 1.6	10.2 ± 4.8	5.0 ± 3.2	7.3 ± 6.9	6.3 ± 4.0	2.8 ± 2.3	2.5 ± 2.8	4.3 ± 4.7	1.0 ± 1.1
	Z3	3.7 ± 1.2	9.8 ± 8.7	5.0 ± 1.4	5.8 ± 2.3	8.3 ± 3.1	6.4 ± 5.2	4.2 ± 4.2	5.3 ± 2.1	7.6 ± 8.6	3.2 ± 2.9	7.8 ± 11.4	3.3 ± 3.7
	Z4	4.2 ± 2.2	6.6 ± 2.7	5.2 ± 2.6	4.8 ± 1.9	8.5 ± 7.0	6.6 ± 4.8	5.3 ± 2.2	7.5 ± 2.6	6.0 ± 3.7	5.2 ± 4.8	6.5 ± 7.3	4.2 ± 7.9
LP&P cells	Z1	72.0 ± 165.6	10.6 ± 15.2	12.0 ± 21.8	13.7 ± 14.9	22.0 ± 38.7	17.8 ± 37.6	3.5 ± 3.2	2.5 ± 5.0	1.8 ± 3.0	0.7 ± 1.6	3.8 ± 5.3	1.0 ± 2.5
	Z2	3.5 ± 7.2	8.8 ± 13.0	13.3 ± 13.6	8.5 ± 7.6	4.3 ± 4.8	4.6 ± 7.6	5.5 ± 8.1	17.5 ± 35.0	0.6 ± 1.3	1.7 ± 2.7	2.7 ± 2.3	1.7 ± 2.1
	Z3	2.7 ± 4.5	8.8 ± 11.1	10.5 ± 7.2	9.5 ± 8.8	2.2 ± 4.0	13.6 ± 19.1	5.8 ± 9.8	0.5 ± 1.0	0.4 ± 0.9	3.8 ± 4.9	5.2 ± 5.0	3.2 ± 4.7
	Z4	3.7 ± 5.0	9.4 ± 11.0	3.2 ± 3.8	5.8 ± 6.3	0.3 ± 0.8	8.2 ± 10.6	9.8 ± 13.6	2.3 ± 2.6	0.6 ± 1.3	4.8 ± 6.0	13.8 ± 18.7	6.5 ± 8.4

at a temperature (900 °C) at which α-TCP should readily convert to β-TCP (Chan *et al.*, 2012). Therefore, at the end, the study design was not as good as expected, but there was still a clear difference of microporosity and grain size between the four scaffold types (Fig. 1, Fig. 2, Fig. 3, Fig. 4, Table 2, Table 3). In addition, the groups with low/high microporosity and small/large granule size had similar values.

Quantitatively, both grain size and microporosity varied threefold, which is at the lower end of what other authors have done in the past. For example, Gauthier *et al.* (Gauthier *et al.*, 1999) varied their grain size from ≈ 0.1-0.2 μm to ≈ 1 μm (Table 1). Hong *et al.* (Hong *et al.*, 2010) used a tenfold variation of grain size. Campion *et al.* (Campion *et al.*, 2011) studied the effect of a twofold change of the strut (micro)porosity (23 to 46 %) on the *in vivo* performance of a silicon-substituted hydroxyapatite. For Coathup *et al.* (Coathup *et al.*, 2012), the range was slightly larger (from 10 to 30 %). As a last example, Klein *et al.* (Klein *et al.*, 1983; Klein *et al.*, 1985; Klein *et al.*, 1986) varied the microporosity over a wider range (in one case from 2 to 60 %), but other architectural parameters were also affected such as the total porosity. Overall, it was believed that the architectural differences of the four groups tested in this study would be large enough to see significant differences in the selected animal model, in particular also because all 4 implant types belonged to a factorial design of experiment (large statistical power).

Despite the care taken to control the composition of the different scaffolds, one group contained α-TCP (Table 2) and minor changes of composition (in particular K and Mg contents) were observed due to the addition of flour (not shown here). In both cases, it is difficult to assess the potential effect on the biological response. Nevertheless, it is important to mention that α-TCP is expected to convert to calcium-deficient hydroxyapatite (CDHA) once implanted, and that CDHA has a solubility very close to that of β-TCP

(Driessens and Verbeeck, 1990; Liu *et al.*, 1999). In addition, there is evidence showing that the composition does not play much of a role in the present animal model and that α-TCP and β-TCP have similar *in vivo* behaviours (Wiltfang *et al.*, 2002).

Scaffold characterisation
Considering the large number of structural factors that have been suggested to affect the *in vivo* response of resorbable scaffolds, it appeared important to perform a very thorough analysis of the scaffold architecture before implantation. This explains why five methods (weighing, materialography, Hg porosimetry, μCT, and N_2 adsorption) were used to characterise the porous space (*e.g.*, porosity and pore size) as well as the solid phase (*e.g.*, grain size, specific surface area).

Total porosity
The two methods used to determine the total scaffold porosity had strong limitations: μCT can only detect pores larger than the resolution (10 μm here) and the type of Hg porosimetry used in the present study can only detect pores smaller than 100 μm. Therefore, the total porosity could only be measured accurately by weighing and materialography. The last two methods gave similar trends: the high microporosity samples had higher porosities than the low microporosity samples, and the highest porosities were measured for the Mg group (Table 2). Even though the correlation coefficient (r^2) between these two methods was superior to 97 %, the porosity values obtained by weighing were significantly higher than those obtained by materialography. This could be related to an overestimation of the sample height and diameter used to calculate the sample volume, or to an underestimation of the sample weight due to surface irregularities. The results obtained by Hg porosimetry were very close to those obtained by weighing and materialography (Table 2). The correlation

coefficient was superior to 94 % when comparing Hg porosimetry results with weighing and materialography results. This high correlation is surprising because with the method settings selected for this study, Hg porosimetry only detected pores smaller than 100 μm, which suggest that most macropores were only accessible from the block outer surface through pores smaller than 100 μm. Therefore, it can be concluded that the total porosity of all groups was in the range of 75 -83 %. These values are similar to values previously reported in the literature for β-TCP bone graft substitutes (Walsh *et al.*, 2003; Bohner *et al.*, 2005; Bai *et al.*, 2010; Feng *et al.*, 2011).

Macroporosity

In the medical field, macropores are defined as pores large enough to allow bone ingrowth. The exact size is still matter of debate, but most agree that the value should be close to 50 μm (Lu *et al.*, 1999; Karageorgiou and Kaplan, 2005; Bohner *et al.*, 2011; Chan *et al.*, 2012). Therefore, a threshold value of 50 μm was used in the two methods allowing the determination of the pore size distribution, namely μCT and Hg porosimetry. The results showed that these two methods gave very different results, in particular for the small grain samples (mg and Mg): Hg porosimetry gave macroporosity values of 11 ± 3 % and 22 ± 10 % for samples mg and Mg, respectively, whereas these values were 54 ± 2 % and 50 ± 3 % using μCT (Table 2). However, there is a fundamental difference between both methods. When a given macropore is inside the scaffold, which is the case for the majority of the macropores (Fig. 3), Hg porosimetry attributes a size, which corresponds to the diameter of the smallest interconnection leading to this macropore. The pore is then referred to be an ink-bottle pore (Van Garderen *et al.*, 2012). To determine the ink-bottle porosity, multicycle Hg intrusion was used. The values measured for the four scaffold types were very close to the total porosity, suggesting that most of the pores have a ink-bottle shape, which is not surprising when looking at the SEM images (Fig. 1-3).

Beside μCT and Hg porosimetry, materialography was also used to assess the macroporosity. However, since it is not possible to determine precisely the pore size based on 2D images, macroporosity could only be estimated as the surface area of "large pores", *i.e.* all pores that could be clearly defined in Fig. 1. Whereas such a definition was fairly easy to apply for mg and mG samples, it became much more difficult for the scaffolds produced with wheat flour (Mg) and particularly for those produced with wheat flour and large grains (MG; Fig. 1). This may explain why the latter value (48 ± 7 %) was quite low compared to the other values (all between 61 ± 4 and 65 ± 4 %; Table 2). In general, the values obtained by materialography were close to the values obtained by μCT (between 50 ± 3 % for Mg and MG, and 56 ± 2 % for mG). So, it can be stated that the macroporosity of four scaffold types was in a similar range (50-65 %), and that most of the macropores in small grain samples were not accessible through 50 μm large channels but through micropores, as indicated by the low macroporosity values measured by Hg porosimetry for these samples (11 ± 3 % for mg samples, and 22 ± 10 % for Mg samples; Table 2).

Macropore size

The mean macropore size could not be quantified accurately because of the limitations of the various characterisation methods. However, since pores smaller than the voxel size (10 μm) cannot be detected by μCT, the mean pore sizes determined by μCT can be considered to give an estimate of the mean macropore size. The values were comprised between 122 ± 2 μm (MG group) and 169 ± 10 μm (mg group) (Table 3). These values are in agreement with the SEM images (Fig 1).

The determination of the link between macropore size and *in vivo* response of a scaffold has been the subject of intensive research. In their review article, Karageorgiou and Kaplan (Karageorgiou and Kaplan, 2005) came to the conclusion that macropores should be larger than 100 μm, most preferably larger than 300 μm to enhance "new bone formation and the formation of capillaries". They also mentioned the need to have pore interconnections, particularly with a diameter larger than 100 μm. Here, the mean macropore sizes were at the lower end of the preferred range and the number of interconnections was limited. However, all four investigated scaffolds fulfilled their bone substitution function, *i.e.* were resorbed and replaced by new bone. In addition, bone was also found in the micropores of all four scaffold types (Fig. 7), suggesting that the walls of non-interconnected macropores could still be invaded by bone.

Microporosity

Three methods were used to assess the sample microporosity: materialography, Hg porosimetry, and μCT. Unfortunately, each of these methods has limitations. For example, pores smaller than the voxel size (10 μm) cannot be detected by μCT. Furthermore, Hg porosimetry consider ink-bottle macropores as micropores if the neck size is in the micro range. Finally, materialography can only give an estimate of the pore cross-sections. However, each of the three methods revealed a significantly higher microporosity for scaffolds designed to have a high microporosity (*i.e.*, samples Mg and MG) (Table 2, Fig. 3, Fig. 4). Looking at materialography and μCT results, this difference was roughly twofold.

Most *in vivo* studies devoted to β-TCP scaffolds do not report the amount and/or size of micropores (Klein *et al.*, 1983; Klein *et al.*, 1985; Klein *et al.*, 1986; Walsh *et al.*, 2003; Bohner *et al.*, 2005; Bai *et al.*, 2010; Feng *et al.*, 2011), making comparisons difficult. Nevertheless, Yuan *et al.* (Yuan *et al.*, 2010) studied microporous calcium phosphate granules containing between 3 and 49 % microporosity (as determined by SEM image analysis). Here, the porosity of the microporous regions, as determined by materialography, was comprised between 21 and 56 % (Table 2). Yuan *et al.* (Yuan *et al.*, 2010) did not measure the micropore and grain size but the values that can be inferred from their SEM images are in a range (1-10 μm) close to those of scaffolds mg to MG (Table 3). In another study, Bohner *et al.* (Bohner *et al.*, 2005) considered macroporous scaffolds containing about 20 % microporosity. Again, these values are similar to those reported here (10 to 30 %; Table 2).

To conclude this section on scaffold characterisation, it can be stated that the four scaffold architectures tested here had morphological features similar to those of many scaffolds presented in the literature. Unfortunately, it was not possible to reach a perfect control of the scaffold architecture. Finally, the differences observed between the different characterisation methods underline the difficulty to quantify architectural features (Bohner *et al.*, 2011).

In vivo results

In the scientific literature, few studies have addressed the effect of grain size and microporosity, in particular on resorbable materials (Table 1). Gauthier *et al*. (Gauthier *et al.*, 1999) found a fourfold increase of resorption rate of BCP scaffolds with a five to ten fold increase of grain size. However, they attributed this increase to the presence of calcium oxide impurities and a "more intimate mixture and stable ultrastructure". No difference of bone formation was noticed. Hong *et al*. (Hong *et al.*, 2010) observed a 10-20 % increase in bone formation with a nine fold increase of grain size. Klein *et al*. (Klein *et al.*, 1983; Klein *et al.*, 1984; Klein *et al.*, 1985; Klein *et al.*, 1986) performed several studies to investigate the effect of microporosity on the *in vivo* behaviour of β-TCP scaffolds. They concluded that a higher microporosity increased the resorption rate, but results were mostly qualitative. More recently, Yokozeki *et al*. (Yokozeki *et al.*, 1998) showed that the addition of micropores into a β-TCP scaffold increased resorption, but no XRD data showing conclusively the nature of the calcium phosphate was presented despite the unusually slow sample resorption (for β-TCP). Furthermore, no explanation was provided to explain the high SSA value of the dense samples (2 m^2/g; current study: between 0.37 ± 0.02 to 0.79 ± 0.08 m^2/g; Table 3). This survey shows that the results presented in the literature are sometimes contradictory.

By conducting the present systematic study, it was hoped that clearer conclusions could be drawn regarding the effect of microporosity and grain size, but hardly any difference could be detected between the four sample types. One may argue that the animal model used here is not sensitive enough to test osteoconduction. However, in this model, empty defects are filled with fat and fibrous tissue and only *ca*. 20 % bone forms at the defect edges (Nuss *et al.*, 2006). Since the defects are not subjected to mechanical loading, the formation of fibrous tissue cannot be attributed to a mechanical stability. Combining these two observations reveal that the presence of a bone substitute in the defect is essential for its regeneration and one may talk about "critical-size defects". Obviously, other models could have been considered, such as maxillofacial onlay models or spine postero-lateral fusion models. It is possible that the conclusions could have been different. However, our goal was to test bone substitutes in a model that is relevant for orthopaedic applications. Also, it allowed direct comparison between results of different *in vivo* studies. Importantly, there is to our knowledge no scientific publication linking animal model (specie, location) and study outcome. It is true that some models seem to be very sensitive (*e.g.*, ectopic models (Yuan *et al.*, 2010)), but

there are few data showing their relevance for orthotopic locations.

Regarding the absence of significant differences between tested scaffolds, one may also argue that the three-fold change of microporosity and grain size was too limited to produce significant results. However, Campion *et al*. (Campion *et al.*, 2011) (twofold change of microporosity) and Coathup *et al*. (Coathup *et al.*, 2012) (three-fold change of microporosity) observed highly significant effects. Moreover, even though the number of experimental repeats ($n = 6$) was below the number generally recommended in standardised animal tests ($n = 8$), the experiments were performed according to a factorial design of experiment. Therefore, the standard deviation of each experimental group was not only calculated from the results of 6 experiments, but the results of 72 experiments. As such, the statistical power of the present study was much higher than with $n = 8$. The second explanation for the absence of significant differences is that the biological response was not affected by the physical changes of the scaffolds. Results presented in the literature suggest indeed that the biological response of bone substitutes has a low sensitivity to physico-chemical changes. For example, many materials have been successful as bone substitute, despite a broad range of solubility and resorption mechanism. Focusing on architecture, Lu *et al*. (Lu *et al.*, 1999) explained this low sensitivity to the geometric changes occurring during resorption. Okuda *et al*. (Okuda *et al.*, 2007) proposed that "the bioresorbability of the bone substitute (…) affects the metabolism of the subsequently formed bone tissue". Metsger (Metsger *et al.*, 1993) noticed that "there appears to be a critical time during which resorption and bone ingrowth are accelerated at a faster rate". Later, this author wrote that "there is a trend for implants of both pore size distributions to increase simultaneously in volume porosity and bone ingrowth". Cancedda's group (Mastrogiacomo *et al.*, 2007; Papadimitropoulos *et al.*, 2007) went a step further and postulated that there is a coupling between ceramic resorption and bone formation. This idea was then used by Bashoor-Zadeh *et al*. (Bashoor-Zadeh *et al.*, 2011) to explain why the resorption rate of β-TCP scaffolds did not vary despite large changes of macropore size (from 150 to 1200 μm). The coupling between scaffold resorption and bone formation could explain the strong correlation seen in this study between ceramic content and bone volume ($r^2 = 0.85$; Fig. 8d).

To explore the coupling mechanism between resorption, bone formation and scaffold in more detail, all results obtained with the present animal model and resorbable bone graft substitutes varying in composition (monetite, brushite, β-TCP, apatite, gypsum) and formulations (scaffolds, cements) were computed and plotted together (Fig 12). The main observation is that all resorption and bone formation results are fairly similar, despite changes in solubility over several order of magnitudes (*e.g.*, between gypsum and hydroxyapatite) and significant changes in architecture (from sub-microporous for apatite cements to macroporous). Indeed, the bone substitute fraction varied between 0 % and 70 % of the initial amount at two months (Fig. 12a), whereas the bone fraction varied between 20

and 50 % (Fig. 12b). This finding suggests that there is a very strong coupling between implant resorption and bone formation. This could be related to the fact that calcium and phosphate ions, which are temporarily released during calcium phosphate resorption *via* dissolution (Koerten and van der Meulen, 1999), are known to regulate bone cell metabolism (Zaidi *et al.*, 1989; Meleti *et al.*, 2000; Wu *et al.*, 2003). In addition, there is evidence that phosphate ions can act as an osteoinductive substance (Habibovic *et al.*, 2010). Summarising the results obtained with various calcium phosphate bone graft substitutes in the sheep model used in this study, it appears that the biological response of calcium phosphate bone graft substitutes is very moderately affected by their architecture and chemical composition. In Fig. 12, the only underperforming materials were poorly-resorbable dense materials such as apatite cements: their resorption rate was low, hence limiting bone formation. Nevertheless, the sheep model considered here is a so-called 5-wall defect in cancellous bone. Other conclusions might be drawn if the samples had been implanted in more open defects (Misch and Dietsh, 1993). The latter defects are typically found in the dental field, where hydroxyapatite-based materials are still the most-used bone substitutes (which does not necessarily mean that they are the best materials). The conclusions drawn from this study cannot be generalised, but underline the need to consider critically the outcome of animal studies.

A few years ago, Lan Levengood *et al.* (Lan Levengood *et al.*, 2010) looked at the effect of micropores on the *in vivo* response of biphasic calcium phosphates. They observed extensive bone formation within the microporous space despite the fact that it is generally agreed that bone invasion requires pore interconnections of at least 100 μm (Karageorgiou and Kaplan, 2005). These authors talked about "multiscale osteointegration" and "paradigm shift". Their results can be related to the work done on microporous β-TCP "plugs" by Mayr *et al.* (Mayr *et al.*, 2007; Mayr *et al.*, 2009; Bernstein *et al.*, 2013; Mayr *et al.*, 2013) showing that micropores can be invaded by bone and that the plugs – despite the absence of macropores – can be rapidly resorbed and replaced by new bone. Other authors made similar observations (Hing *et al.*, 2005; Hing *et al.*, 2007). Here, the presence of blue-stained tissues within the micropores of the four scaffolds support these observations.

Logically, bone invasion into the microporous space should be a function of the size of the interconnections between micropores. Indeed, bone matrix deposition is the result of a cellular process, so the absence of cell invasion should preclude any bone formation in the microporous space. In a recent study, Polak *et al.* (Polak *et al.*, 2013) studied the penetration depth of cells into a microporous ceramic and could relate the results to the size and stiffness of the tested cells. Interestingly, these authors showed that cells could invade micropores through pore interconnections smaller than their diameter. The importance of cell penetration could explain why there is, to our knowledge, no study reporting bone invasion into apatite cements, materials that are characterised by sub-μm to nm scale pore interconnections (Espanol *et al.*, 2009). In the present study, not only the microporosity

but also the micropore size varied threefold. Two scaffold types contained sub-μm pore interconnections (Fig 2-4), well below bone-relevant cell sizes (4-12 μm; (Polak *et al.*, 2013)). Nevertheless, blue-stained tissue invasion was observed in all 4 sample types (Fig. 7). Transmission electron microscopy images will have to be taken and other staining will have to be done to confirm the formation of mineralised collagen and cells in the microporous space.

Conclusion

Four types of β-TCP scaffolds were produced with the same macropore size (≈ 150 μm) and total porosity (≈ 80 %), but various microporosities (from 10 to 30 %) and grain sizes (from 1.3 to 3.4 μm). As a result, the four groups were considered to be part of a factorial design of experiments comprising two factors (microporosity and grain size) and two levels (low and high). The samples architecture was characterised according to different methods, such as geometrical density, materialography, Hg porosimetry, μCT, and nitrogen adsorption. The results demonstrated that the design was not perfect, but certainly sufficient to draw conclusions about the two investigated factors. Six samples of each group were implanted in a sheep model for 2, 4 and 8 weeks, leading to a total of 72 samples. The histological, histomorphometrical, and μCT analysis revealed no difference of bone formation between the different groups. The only significant factor at $p < 0.01$ was an increase of resorption and fibrous tissue formation with an increase of microporosity between 4 and 8 weeks implantation. Considering the three-fold difference in grain size and microporosity between the different scaffolds, these results suggest that the biological mechanisms controlling healing are highly regulated, and that the *in vivo* performance of scaffolds implanted in the present animal model are mostly limited by biology rather than scaffold design. This conclusion is supported by the results obtained in the same animal model but with non-macroporous and macroporous scaffolds made of materials varying in solubility over several degrees of magnitude (from gypsum to apatite cement, *via* monetite scaffolds). Provided the material is not inert or readily soluble, ceramic resorption and bone formation occur always more or less at the same rate in this particular 5-wall sheep model defect, fairly independently of architecture and composition. The conclusions drawn from this study cannot be generalised, but underline the need to consider critically the outcome of animal studies. Also, the presence of blue-stained tissues within the micropores regions suggest that an in-depth microstructural study has to be performed to better understand the mechanisms of ceramic resorption and bone formation in microporous β-TCP bone substitutes.

References

Apelt D, Theiss F, El-Warrak AO, Zlinszky K, Bettschart-Wolfisberger R, Bohner M, Matter S, Auer JA, von Rechenberg B (2004) *In vivo* behavior of three different injectable hydraulic calcium phosphate cements. Biomaterials **25**: 1439-1451.

Ayers RA, Simske SJ, Bateman TA, Petkus A, Sachdeva RL, Gyunter VE (1999) Effect of nitinol implant porosity on cranial bone ingrowth and apposition after 6 weeks. J Biomed Mater Res **45**: 42-47.

Bai F, Wang Z, Lu J, Liu J, Chen G, Lv R, Wang J, Lin K, Zhang J, Huang X (2010) The correlation between the internal structure and vascularization of controllable porous bioceramic materials *in vivo*: A quantitative study. Tissue Eng A **16**: 3791-3803.

Bashoor-Zadeh M, Baroud G, Bohner M (2011) Simulation of the *in vivo* resorption rate of beta-tricalcium phosphate bone graft substitutes implanted in a sheep model. Biomaterials **32**: 6362-6373.

Basle MF, Chappard D, Grizon F, Filmon R, Delecrin J, Daculsi G, Rebel A (1993) Osteoclastic resorption of Ca-P biomaterials implanted in rabbit bone. Calc Tissue Int **53**: 348-356.

Bernstein A, Niemeyer P, Salzmann G, Südkamp NP, Hube R, Klehm J, Menzel M, Von Eisenhart-Rothe R, Bohner M, Görz L, Mayr HO (2013) Microporous calcium phosphate ceramics as tissue engineering scaffolds for the repair of osteochondral defects: Histological results. Acta Biomater **9**: 7490-7505.

Bobyn JD, Stackpool GJ, Hacking SA, Tanzer M, Krygier JJ (1999) Characteristics of bone ingrowth and interface mechanics of a new porous tantalum biomaterial. J Bone Joint Surg Br **81**: 907-914.

Bohner M, Baumgart F (2004) Theoretical model to determine the effects of geometrical factors on the resorption of calcium phosphate bone substitutes. Biomaterials **25**: 3569-3582.

Bohner M, Loosli Y, Baroud G, Lacroix D (2011) Deciphering the link between architecture and biological response of a bone graft substitute. Acta Biomater **7**: 478-484.

Bohner M, Luginbuhl R, Reber C, Doebelin N, Baroud G, Conforto E (2009) A physical approach to modify the hydraulic reactivity of alpha-tricalcium phosphate powder. Acta Biomater **5**: 3524-3535.

Bohner M, van Lenthe GH, Grunenfelder S, Hirsiger W, Evison R, Muller R (2005) Synthesis and characterization of porous beta-tricalcium phosphate blocks. Biomaterials.

Bose S, Fielding G, Tarafder S, Bandyopadhyay A (2013) Understanding of dopant-induced osteogenesis and angiogenesis in calcium phosphate ceramics. Trends Biotech **31**: 594-605.

Campion CR, Chander C, Buckland T, Hing K (2011) Increasing strut porosity in silicate-substituted calcium-phosphate bone graft substitutes enhances osteogenesis. J Biomed Mater Res B Appl Biomater **97 B**: 245-254.

Chan O, Coathup MJ, Nesbitt A, Ho CY, Hing KA, Buckland T, Campion C, Blunn GW (2012) The effects of microporosity on osteoinduction of calcium phosphate

bone graft substitute biomaterials. Acta Biomater **8**: 2788-2794.

Chen IW, Wang XH (2000) Sintering dense nanocrystalline ceramics without final-stage grain growth. Nature **404**: 168-171.

Chen PL, Chen IW (1996) Sintering of fine oxide powders: I, microstructural evolution. J Am Ceram Soc **79**: 3129-3141.

Chen PL, Chen IW (1997) Sintering of fine oxide powders: II, sintering mechanisms. J Am Ceram Soc **80**: 637-645.

Coathup MJ, Hing KA, Samizadeh S, Chan O, Fang YS, Campion C, Buckland T, Blunn GW (2012) Effect of increased strut porosity of calcium phosphate bone graft substitute biomaterials on osteoinduction. J Biomed Mater Res A **100 A**: 1550-1555.

Daculsi G, Passuti N (1990) Effect of the macroporosity for osseous substitution of calcium phosphate ceramics. Biomaterials **11**: 86-87.

De Groot K (1988) Effect of porosity and physicochemical properties on the stability, resorption, and strength of calcium phosphate ceramics. Ann N Y Acad Sci **523**: 227-233.

De Groot K, Tencer A, Waite P, Nichols J, Kay J (1988) Significance of the porosity and physical chemistry of calcium phosphate ceramics. Dental and other head and neck uses. Ann N Y Acad Sci **523**: 272-277.

Driessens FCM, Verbeeck RMH (1990) Biominerals. CRC Press, Boca Raton.

Eggli PS, Muller W, Schenk RK (1988) Porous hydroxyapatite and tricalcium phosphate cylinders with two different pore size ranges implanted in the cancellous bone of rabbits. A comparative histomorphometric and histologic study of bony ingrowth and implant substitution. Clin Orthop **232**: 127-138.

Engelhardt P, Gasser JA (1995) LEICA HistoDur: A resin specifically designed for the histology of mineralized tissues. (Ltd SP, ed), Leica Applications Brief, Basel.

Espanol M, Perez RA, Montufar EB, Marichal C, Sacco A, Ginebra MP (2009) Intrinsic porosity of calcium phosphate cements and its significance for drug delivery and tissue engineering applications. Acta Biomater **5**: 2752-2762.

Feng B, Jinkang Z, Zhen W, Jianxi L, Jiang C, Jian L, Guolin M, Xin D (2011) The effect of pore size on tissue ingrowth and neovascularization in porous bioceramics of controlled architecture *in vivo*. Biomed Mater **6**: 015007.

Flautre B, Descamps M, Delecourt C, Blary MC, Hardouin P (2001) Porous HA ceramic for bone replacement: role of the pores and interconnections - experimental study in the rabbit. J Mater Sci Mater Med **12**: 679-682.

Gauthier O, Bouler JM, Aguado E, Legeros RZ, Pilet P, Daculsi G (1999) Elaboration conditions influence physicochemical properties and *in vivo* bioactivity of macroporous biphasic calcium phosphate ceramics. J Mater Sci Mater Med **10**: 199-204.

Gogolewski S, Gorna K, Zaczynska E, Czarny A (2008) Structure-property relations and cytotoxicity of isosorbide-based biodegradable polyurethane scaffolds

for tissue repair and regeneration. J Biomed Mater Res A **85**: 456-465.

Habibovic P, Bassett DC, Doillon CJ, Gerard C, McKee MD, Barralet JE (2010) Collagen biomineralization *in vivo* by sustained release of inorganic phosphate ions. Adv Mater **22**: 1858-1862.

Haugen HJ, Monjo M, Rubert M, Verket A, Lyngstadaas SP, Ellingsen JE, Rønold HJ, Wohlfahrt JC (2013) Porous ceramic titanium dioxide scaffolds promote bone formation in rabbit peri-implant cortical defect model. Acta Biomater **9**: 5390-5399.

Hench LL (2006) The story of Bioglass. J Mater Sci Mater Med **17**: 967-978.

Hildebrand T, Laib A, Muller R, Dequeker J, Ruegsegger P (1999) Direct three-dimensional morphometric analysis of human cancellous bone: microstructural data from spine, femur, iliac crest, and calcaneus. J Bone Miner Res **14**: 1167-1174.

Hing KA, Annaz B, Saeed S, Revell PA, Buckland T (2005) Microporosity enhances bioactivity of synthetic bone graft substitutes. J Mater Sci Mater Med **16**: 467-475.

Hing KA, Wilson LF, Buckland T (2007) Comparative performance of three ceramic bone graft substitutes. Spine J **7**: 475-490.

Hong Y, Fan H, Li B, Guo B, Liu M, Zhang X (2010) Fabrication, biological effects, and medical applications of calcium phosphate nanoceramics. Mater Sci Eng R **70**: 225-242.

Hutmacher DW (2000) Scaffolds in tissue engineering bone and cartilage. Biomaterials **21**: 2529-2543.

Ignatius AA, Betz O, Augat P, Claes LE (2001) *In vivo* investigations on composites made of resorbable ceramics and poly(lactide) used as bone graft substitutes. J Biomed Mater Res **58**: 701-709.

Ishaug-Riley SL, Crane GM, Gurlek A, Miller MJ, Yasko AW, Yaszemski MJ, Mikos AG (1997) Ectopic bone formation by marrow stromal osteoblast transplantation using poly(DL-lactic-co-glycolic acid) foams implanted into the rat mesentery. J Biomed Mater Res **36**: 1-8.

Itala AI, Ylanen HO, Ekholm C, Karlsson KH, Aro HT (2001) Pore diameter of more than 100 microns is not requisite for bone ingrowth in rabbits. J Biomed Mater Res **58**: 679-683.

Jones JR, Hench LL (2004) Factors affecting the structure and properties of bioactive foam scaffolds for tissue engineering. J Biomed Mater Res B Appl Biomater **68B**: 36-44.

Karageorgiou V, Kaplan D (2005) Porosity of 3D biomaterial scaffolds and osteogenesis. Biomaterials **26**: 5474-5491.

Kasten P, Beyen I, Niemeyer P, Luginbuhl R, Bohner M, Richter W (2008) Porosity and pore size of beta-tricalcium phosphate scaffold can influence protein production and osteogenic differentiation of human mesenchymal stem cells: an *in vitro* and *in vivo* study. Acta Biomater **4**: 1904-1915.

Klawitter JJ, Hulbert SF (1971) Application of porous ceramics for the attachment of load bearing internal orthopedic applications. J Biomed Mater Res Symp **2**: 161-229.

Klein CP, de Groot K, Driessen AA, van der Lubbe HB (1985) Interaction of biodegradable beta-whitlockite ceramics with bone tissue: an *in vivo* study. Biomaterials **6**: 189-192.

Klein CPAT, De Groot K, Driessen AA, Van der Lubbe HBM (1986) A comparative study of different β-whitlockite ceramics in rabbit cortical bone with regard to their biodegradation behaviour. Biomaterials **7**: 144-146.

Klein CPAT, Driessen AA, De Groot K (1984) Relationship between the degradation behaviour of calcium phosphate ceramics and their physical/chemical characteristics and ultrastructural geometry. Biomaterials **5**: 157-160.

Klein CPAT, Driessen AA, De Groot K, Van den Hooff A (1983) Biodegradation behavior of various calcium phosphate materials in bone tissue. J Biomed Mater Res **17**: 769-784.

Koerten HK, van der Meulen J (1999) Degradation of calcium phosphate ceramics. J Biomed Mater Res **44**: 78-86.

Lan Levengood SK, Polak SJ, Wheeler MB, Maki AJ, Clark SG, Jamison RD, Wagoner Johnson AJ (2010) Multiscale osteointegration as a new paradigm for the design of calcium phosphate scaffolds for bone regeneration. Biomaterials **31**: 3552-3563.

Le Nihouannen D, Daculsi G, Saffarzadeh A, Gauthier O, Delplace S, Pilet P, Layrolle P (2005) Ectopic bone formation by microporous calcium phosphate ceramic particles in sheep muscles. Bone **36**: 1086-1093.

LeGeros RZ (1993) Biodegradation and bioresorption of calcium phosphate ceramics. Clin Mater **14**: 65-88.

LeGeros RZ (2002) Properties of osteoconductive biomaterials: calcium phosphates. Clin Orthop: 81-98.

LeGeros RZ, Parsons JR, Daculsi G, Driessens F, Lee D, Liu ST, Metsger S, Peterson D, Walker M (1988) Significance of the porosity and physical chemistry of calcium phosphate ceramics. Biodegradation-bioresorption. Ann N Y Acad Sci **523**: 268-271.

Linhart W, Briem D, Amling M, Rueger JM, Windolf J (2004) Mechanical failure of a porous hydroxyapatite ceramic 7.5 years after treatment of a fracture of the proximal tibia. Unfallchirurg **107**: 154-157.

Liu CS, Shen W, Chen JG (1999) Solution property of calcium phosphate cement hardening body. Mater Chem Phys **58**: 78-82.

Lu JX, Flautre B, Anselme K, Hardouin P, Gallur A, Descamps M, Thierry B (1999) Role of interconnections in porous bioceramics on bone recolonization *in vitro* and *in vivo*. J Mater Sci Mater Med **10**: 111-120.

Malard O, Bouler JM, Guicheux J, Heymann D, Pilet P, Coquard C, Daculsi G (1999) Influence of biphasic calcium phosphate granulometry on bone ingrowth, ceramic resorption, and inflammatory reactions: preliminary *in vitro* and *in vivo* study. J Biomed Mater Res **46**: 103-111.

Mastrogiacomo M, Papadimitropoulos A, Cedola A, Peyrin F, Giannoni P, Pearce SG, Alini M, Giannini C, Guagliardi A, Cancedda R (2007) Engineering of bone using bone marrow stromal cells and a silicon-stabilized tricalcium phosphate bioceramic: evidence for a coupling between bone formation and scaffold resorption. Biomaterials **28**: 1376-1384.

Mathew M, Schroeder LW, Dickens B, Brown WE (1977) The crystal structure of a-Ca3(PO4)2. Acta Cryst **B33**: 1325-1333.

Mayr HO, Dietrich M, Fraedrich F, Hube R, Nerlich A, von Eisenhart-Rothe R, Hein W, Bernstein A (2009) Microporous pure beta-tricalcium phosphate implants for press-fit fixation of anterior cruciate ligament grafts: strength and healing in a sheep model. Arthroscopy **25**: 996-1005.

Mayr HO, Hube R, Bernstein A, Seibt AB, Hein W, von Eisenhart-Rothe R (2007) Beta-tricalcium phosphate plugs for press-fit fixation in ACL reconstruction--a mechanical analysis in bovine bone. Knee **14**: 239-244.

Mayr HO, Klehm J, Schwan S, Hube R, Südkamp NP, Niemeyer P, Salzmann G, Von Eisenhardt-Rothe R, Heilmann A, Bohner M, Bernstein A (2013) Microporous calcium phosphate ceramics as tissue engineering scaffolds for the repair of osteochondral defects: Biomechanical results. Acta Biomater **9**: 4845-4855.

Mazaheri M, Haghighatzadeh M, Zahedi AM, Sadrnezhaad SK (2009) Effect of a novel sintering process on mechanical properties of hydroxyapatite ceramics. J Alloys Comp **471**: 180-184.

Meleti Z, Shapiro IM, Adams CS (2000) Inorganic phosphate induces apoptosis of osteoblast-like cells in culture. Bone **27**: 359-366.

Metsger DS, Arnala I, Faugere MC, Malluche HH (1993) Histomorphometric analysis of tricalcium phosphate ceramic implanted into turkeys. Bone **14**: 243-248.

Misch CE, Dietsh F (1993) Bone-grafting materials in implant dentistry. Implant Dent **2**: 158-167.

Mondrinos MJ, Dembzynski R, Lu L, Byrapogu VKC, Wootton DM, Lelkes PI, Zhou J (2006) Porogen-based solid freeform fabrication of polycaprolactone-calcium phosphate scaffolds for tissue engineering. Biomaterials **27**: 4399-4408.

Murakami Y, Honda Y, Anada T, Shimauchi H, Suzuki O (2010) Comparative study on bone regeneration by synthetic octacalcium phosphate with various granule sizes. Acta Biomater **6**: 1542-1548.

Nuss KM, Auer JA, Boos A, von Rechenberg B (2006) An animal model in sheep for biocompatibility testing of biomaterials in cancellous bones. BMC Musculoskelet Disord **7**: 67.

Oberle A, Theiss F, Bohner M, Muller J, Kastner SB, Frei C, Boecken I, Zlinszky K, Wunderlin S, Auer JA, von Rechenberg B (2005) [Investigation about the clinical use of brushite- and hydroxylapatite-cement in sheep]. Schw Arch Tierheilkunde **147**: 482-490.

Okuda T, Ioku K, Yonezawa I, Minagi H, Kawachi G, Gonda Y, Murayama H, Shibata Y, Minami S, Kamihira S, Kurosawa H, Ikeda T (2007) The effect of the microstructure of beta-tricalcium phosphate on the metabolism of subsequently formed bone tissue. Biomaterials **28**: 2612-2621.

Papadimitropoulos A, Mastrogiacomo M, Peyrin F, Molinari E, Komlev VS, Rustichelli F, Cancedda R (2007) Kinetics of *in vivo* bone deposition by bone marrow stromal cells within a resorbable porous calcium phosphate scaffold: An X-ray computed microtomography study. Biotech Bioeng **98**: 271-281.

Polak SJ, Levengood SKL, Wheeler MB, Maki AJ, Clark SG, Johnson AJW (2011) Analysis of the roles of microporosity and BMP-2 on multiple measures of bone regeneration and healing in calcium phosphate scaffolds. Acta Biomater **7**: 1760-1771.

Polak SJ, Rustom LE, Genin GM, Talcott M, Wagoner Johnson AJ (2013) A mechanism for effective cell-seeding in rigid, microporous substrates. Acta Biomater.

Rodriguez-Carvajal J (2001) Recent Developments of the Program FULLPROF. Commission on Powder Diffraction (IUCr) Newsletter **26**: 12-19.

Schliephake H, Neukam FW, Klosa D (1991) Influence of pore dimensions on bone ingrowth into porous hydroxylapatite blocks used as bone graft substitutes. A histometric study. Int J Oral Maxillofac Surg **20**: 53-58.

Schroeder LW, Dickens B, Brown WE (1977) Crystallographic studies of the role of Mg as a stabilizing impurity in b-Ca$_3$(PO$_4$)$_2$. II. Refinement of Mg-containing b-Ca$_3$(PO$_4$)$_2$. J Solid State Chem **22**: 253-262.

Sridharan G, Shankar AA (2012) Toluidine blue: A review of its chemistry and clinical utility. J Oral Maxillofac Pathol **16**: 251-255.

Sudarsanan K, Young RA (1969) Significant precision in crystal structure details: Holly springs hydroxyapatite. Acta Cryst **B25**: 1534-1543.

Theiss F, Apelt D, Brand B, Kutter A, Zlinszky K, Bohner M, Matter S, Frei C, Auer JA, von Rechenberg B (2005) Biocompatibility and resorption of a brushite calcium phosphate cement. Biomaterials **26**: 4383-4394.

Van Blitterswijk CA, Grote JJ, Kuijpers W, Daems WT, de Groot K (1986) Macropore tissue ingrowth: a quantitative and qualitative study on hydroxyapatite ceramic. Biomaterials **7**: 137-143.

Van der Meulen J, Koerten HK (1994) Inflammatory response and degradation of three types of calcium phosphate ceramic in a non-osseous environment. J Biomed Mater Res **28**: 1455-1463.

Van Garderen N, Clemens FJ, Kaufmann J, Urbanek M, Binkowski M, Graule T, Aneziris CG (2012) Pore analyses of highly porous diatomite and clay based materials for fluidized bed reactors. Micropor Mesopor Mater **151**: 255-263.

Vert M (2007) Polymeric biomaterials: Strategies of the past *vs*. strategies of the future. Progr Polymer Sci **32**: 755-761.

Von Doernberg MC, von Rechenberg B, Bohner M, Grunenfelder S, van Lenthe GH, Muller R, Gasser B, Mathys R, Baroud G, Auer J (2006) *In vivo* behavior of calcium phosphate scaffolds with four different pore sizes. Biomaterials **27**: 5186-5198.

Von Rechenberg B, Génot OR, Nuss KM, Galuppo L, Fulmer M, Jacobson E, Kronen P, Zlinszky K, Auer JA (2013) Evaluation of four biodegradable, injectable bone cements in an experimental drill hole model in sheep. Eur J Pharma Biopharm **85**: 130-138.

Walsh WR, Morberg P, Yu Y, Yang JL, Haggard W, Sheath PC, Svehla M, Bruce WJ (2003) Response of a calcium sulfate bone graft substitute in a confined cancellous defect. Clin Orthop **406**: 228-236.

Wei J, Jia J, Wu F, Wei S, Zhou H, Zhang H, Shin JW, Liu C (2010) Hierarchically microporous/macroporous scaffold of magnesium-calcium phosphate for bone tissue regeneration. Biomaterials **31**: 1260-1269.

Wiltfang J, Merten HA, Schlegel KA, Schultze-Mosgau S, Kloss FR, Rupprecht S, Kessler P (2002) Degradation characteristics of alpha and beta tri-calcium-phosphate (TCP) in minipigs. J Biomed Mater Res **63**: 115-121.

Witte F, Ulrich H, Palm C, Willbold E (2007) Biodegradable magnesium scaffolds: Part II: Peri-implant bone remodeling. J Biomed Mater Res A **81**: 757-765.

Wu X, Itoh N, Taniguchi T, Nakanishi T, Tanaka K (2003) Requirement of calcium and phosphate ions in expression of sodium-dependent vitamin C transporter 2 and osteopontin in MC3T3-E1 osteoblastic cells. Biochim Biophys Acta Mol Cell Res **1641**: 65-70.

Yokozeki H, Hayashi T, Nakagawa T, Kurosawa H, Shibuya K, Ioku K (1998) Influence of surface microstructure on the reaction of the active ceramics *in vivo*. J Mater Sci Mater Med **9**: 381-384.

Yuan H, Fernandes H, Habibovic P, de Boer J, Barradas AM, de Ruiter A, Walsh WR, van Blitterswijk CA, de Bruijn JD (2010) Osteoinductive ceramics as a synthetic alternative to autologous bone grafting. Proc Natl Acad Sci USA **107**: 13614-13619.

Zaidi M, Datta HK, Patchell A, Moonga B, MacIntyre I (1989) Calcium-activated' intracellular calcium elevation: a novel mechanism of osteoclast regulation. Biochem Biophys Res Commun **163**: 1461-1465.